Atmos. Chem. Phys., 18, 7109–7129, 2018
https://doi.org/10.5194/acp-18-7109-2018
© Author(s) 2018. This work is distributed under
the Creative Commons Attribution 4.0 License.

Atmospheric Chemistry and Physics
Open Access
EGU

Global modelling of the total OH reactivity: investigations on the "missing" OH sink and its atmospheric implications

Valerio Ferracci[1,a], Ines Heimann[1], N. Luke Abraham[1,2], John A. Pyle[1,2], and Alexander T. Archibald[1,2]

[1]Centre for Atmospheric Science, Department of Chemistry, University of Cambridge, Lensfield Road, CB2 1EW, UK
[2]National Centre for Atmospheric Science, University of Cambridge, Cambridge, UK
[a]now at: Centre for Environmental and Agricultural Informatics, Cranfield University, College Road, MK43 0AL, UK

Correspondence: Valerio Ferracci (v.ferracci@cranfield.ac.uk)

Received: 3 January 2018 – Discussion started: 9 January 2018
Revised: 16 April 2018 – Accepted: Accepted on 26 – Published: 24 May 2018

Abstract. The hydroxyl radical (OH) plays a crucial role in the chemistry of the atmosphere as it initiates the removal of most trace gases. A number of field campaigns have observed the presence of a "missing" OH sink in a variety of regions across the planet. A comparison of direct measurements of the OH loss frequency, also known as total OH reactivity (k_{OH}), with the sum of individual known OH sinks (obtained via the simultaneous detection of species such as volatile organic compounds and nitrogen oxides) indicates that, in some cases, up to 80 % of k_{OH} is unaccounted for. In this work, the UM-UKCA chemistry-climate model was used to investigate the wider implications of the missing reactivity on the oxidising capacity of the atmosphere. Simulations of the present-day atmosphere were performed and the model was evaluated against an array of field measurements to verify that the known OH sinks were reproduced well, with a resulting good agreement found for most species. Following this, an additional sink was introduced to simulate the missing OH reactivity as an emission of a hypothetical molecule, X, which undergoes rapid reaction with OH. The magnitude and spatial distribution of this sink were underpinned by observations of the missing reactivity. Model runs showed that the missing reactivity accounted for on average 6 % of the total OH loss flux at the surface and up to 50 % in regions where emissions of the additional sink were high. The lifetime of the hydroxyl radical was reduced by 3 % in the boundary layer, whilst tropospheric methane lifetime increased by 2 % when the additional OH sink was included. As no OH recycling was introduced following the initial oxidation of X, these results can be interpreted as an upper limit of the effects of the missing reactivity on the oxidising capacity of the troposphere. The UM-UKCA simulations also allowed us to establish the atmospheric implications of the newly characterised reactions of peroxy radicals (RO_2) with OH. Whilst the effects of this chemistry on k_{OH} were minor, the reaction of the simplest peroxy radical, CH_3O_2, with OH was found to be a major sink for CH_3O_2 and source of HO_2 over remote regions at the surface and in the free troposphere. Inclusion of this reaction in the model increased tropospheric methane lifetime by up to 3 %, depending on its product branching. Simulations based on the latest kinetic and product information showed that this reaction cannot reconcile models with observations of atmospheric methanol, in contrast to recent suggestions.

1 Introduction

The removal of the vast majority of trace gases emitted into the atmosphere is initiated by reaction with the hydroxyl radical, OH. OH is primarily formed following the reaction of excited oxygen atoms, $O(^1D)$, originating from the photolysis of ozone at short wavelengths, with water:

$$O_3 + h\nu(\lambda < 340\,\text{nm}) \rightarrow O(^1D) + O_2 \quad \text{(R1)}$$

$$O(^1D) + H_2O \rightarrow 2OH. \quad \text{(R2)}$$

OH generated via any route other than Reaction (R1) and Reaction (R2) is referred to as secondary OH; examples of processes yielding secondary OH include the photolysis of H_2O_2 and the reaction of HO_2 with NO. Crucially, OH abundance and availability (and consequently the oxidising capacity of the atmosphere) are governed by the balance between

OH sources (primary and secondary) and sinks, consisting of the totality of the species that react with OH: these include volatile organic compounds (VOCs), nitrogen oxides (NO_x) and many others species, both biogenic and anthropogenic.

In this respect, the total OH loss frequency, also known as the total OH reactivity (k_{OH}), is a useful measure of the total amount of OH sinks present in a particular environment. k_{OH} is defined as the pseudo first-order rate constant for OH loss and is equivalent to the inverse of the OH lifetime, τ_{OH}, as shown in Eq. (1):

$$k_{OH} = \sum_{i=1}^{n} k_{OH+X_i}[X_i] = 1/\tau_{OH}, \quad (1)$$

where $[X_i]$ designates the concentration (usually in molecules cm^{-3}) of OH sink X_i, and k_{OH+X_i} is the rate constant for the reaction of OH with X_i (usually expressed in cm^3 $molecule^{-1}$ s^{-1}). It follows from Eq. (1) that, if the atmospheric abundance of all OH sinks is measured and provided that the rate constants for their reaction with OH are known, k_{OH} can be determined as the sum of the individual sink reactivities.

Over the last two decades, techniques capable of measuring the total OH reactivity directly, without the need to quantify individual sinks, have become available: these rely either on direct measurements of the OH decay rate (Di Carlo et al., 2004; Ingham et al., 2009; Kovacs and Brune, 2001) or on the comparative reactivity method (Sinha et al., 2008), in which k_{OH} is determined from the reactivity of a reference species (typically pyrrole). A review (Yang et al., 2016) recently described these techniques in detail, whilst the various instruments developed for direct measurements of k_{OH} have been the subject of an extensive intercomparison (Fuchs et al., 2017). These techniques, when deployed in the field along with instruments for the detection of trace species, have enabled the comparison of direct measurements of the total k_{OH} with the sum of reactivities of the individual OH sinks. In this respect, measurements of the total OH reactivity can be used to test our understanding of tropospheric oxidation; provided that the totality of OH sinks are accounted for and measured, the sum of individual reactivities and the total k_{OH} should agree.

Field campaigns across the globe have, however, highlighted discrepancies between these two approaches, with most measurements reporting values of the total k_{OH} higher than the sum of the individual reactivities (Yang et al., 2016). These results indicate that a fraction of the total OH reactivity cannot be accounted for: this is often referred to as "missing" reactivity and attributed to a "missing" OH sink. The magnitude of the observed missing reactivity in the literature varies depending on the geographic location of the measurement and the season, but could amount to as much as 80 % of the total k_{OH} as measured by Nölscher et al. (2016) in the Amazon rainforest.

Many studies have attempted to identify the missing sink: whilst some authors have attributed the missing reactivity to the presence of primary emissions that escaped detection (Holzinger et al., 2005; Kaiser et al., 2016; Sinha et al., 2010), others have pointed to the reactions of OH with short-lived oxidation intermediates (Hansen et al., 2014; Nakashima et al., 2014), which are notoriously challenging to measure in the field. Other studies still, including that by Nölscher et al. (2016) in the Amazon rainforest, attributed the missing reactivity to both unidentified biogenic emissions and photooxidation products.

An exponential temperature dependence of the missing reactivity was observed during two campaigns carried out in the same North American forest, consistent with either primary biogenic emissions (Di Carlo et al., 2004) or with their oxidation products (Hansen et al., 2014). Some of the campaigns carried out in other forested environments also observed a similar trend (Kaiser et al., 2016; Mao et al., 2012; Zannoni et al., 2017), whereas others found no evidence for this correlation (Ren et al., 2006b; Sinha et al., 2010).

In an attempt to account for the additional OH reactivity potentially arising from unmeasured oxidation intermediates, a number of studies invoked box modelling to determine the abundance of these species and their contribution to k_{OH}. These efforts have been met with mixed results: whilst some managed to reconcile the total k_{OH} with the sum of reactivities once the oxidation intermediates were taken into account (Whalley et al., 2016), others obtained different degrees of improvement on the agreement between the two, leaving different fractions of k_{OH} still unaccounted for (Edwards et al., 2013; Elshorbany et al., 2012; Kaiser et al., 2016; Kovacs et al., 2003; Lee et al., 2009; Lou et al., 2010; Mao et al., 2012; Mogensen et al., 2011; Yang et al., 2017).

Regardless of its identity, the very presence of an additional OH sink would lead to shorter τ_{OH} in the real atmosphere than in current models; this would, in turn, lead to longer lifetimes for species that are primarily removed by reaction with OH, such as the vast majority of biogenic and anthropogenic VOCs as well as high-impact greenhouse gases such as methane. Given the complex interactions of the OH radical in the photochemistry of the troposphere, global atmospheric modelling provides a powerful tool with which to investigate potential candidates for the missing sink as well as to establish its impacts on the oxidising capacity of the lower atmosphere.

So far only two studies have attempted global modelling of k_{OH}: the focus of these works was either modelling the global OH budget (Lelieveld et al., 2016) or the total reactive organic carbon budget (Safieddine et al., 2017). Detailed comparisons of the modelled k_{OH} with observations or the missing reactivity were not addressed.

This work will make an extensive comparison between modelled k_{OH} and observations, with particular attention to the contribution of individual sinks to the total OH reactivity. Section 3 describes our base integration and discusses a comparison with observations. Sections 4 and 5 tackle the challenge of modelling the missing reactivity using two approaches. Firstly (Sect. 4), we introduce an additional OH

Table 1. Summary of the model runs described in this work.

Run name	Chemistry scheme	Description
Base run	CheST	This run provides a means to assess how well the model captures known OH sinks, i.e. the individual reactivities in the sum term of Eq. (1). It also provides a point of comparison for the runs that follow. The base run is discussed in Sect. 3.
X + OH run	CheST with Reaction (R3)	An additional OH sink, species X, is introduced in the model to account for the missing k_{OH}. This run is described in Sect. 4.
CH_3O_2 + OH run 1	CheST with Reaction (R4)	The multi-channel reaction of methyl peroxy radicals (CH_3O_2) with OH was included in the chemistry scheme with branching ratios $\alpha = 1$, $\gamma = 0$ *. This run is described in Sect. 5.2.
CH_3O_2 + OH run 2	CheST with Reaction (R4)	Same as CH_3O_2 + OH run 1 but with branching ratios $\alpha = 0.8$, $\gamma = 0.2$ *. This run is described in Sect. 5.2.
CH_3O_2 + OH run 3	CheST with Reaction (R4)	Same as CH_3O_2 + OH run 1 but with branching ratios $\alpha = 0.6$, $\gamma = 0.4$ *. This run is described in Sect. 5.2.

* Branching ratios α and γ are defined in Sect. 5.2.

sink, the geographical distribution and abundance of which are underpinned by the observations of missing reactivity available. Secondly (Sect. 5), we include in the model the reactions of peroxy radicals (RO_2) with OH. As this novel RO_2 + OH chemistry has been characterised in the laboratory only in recent years, the role of RO_2 as an OH sink may have been overlooked (Fittschen et al., 2014). The implications of both approaches for the oxidising capacity of the atmosphere are then discussed.

2 Method

State-of-the-art chemistry-climate models have become an extremely important tool in the study of atmospheric science, allowing the exploration of a number of global scenarios with an unprecedented level of detail. However, recent studies have shown that the way the chemistry is implemented in the model (e.g. different oxidation schemes for complex emitted species) can have a major impact on crucial properties of the atmosphere such as the formation of tropospheric ozone (Squire et al., 2015). It is therefore important to validate these models against observations of relevant chemical species whenever possible. In this work, a global chemistry-climate model, the Met Office's Unified Model with the United Kingdom Chemistry and Aerosols scheme, UM-UKCA version 8.4, (Abraham et al., 2012) was used to investigate the total OH reactivity, k_{OH}. The model was run in the N96-L85 configuration, providing a horizontal resolution of 1.875° in longitude × 1.25° in latitude on 85 vertical levels from the surface up to a height of 85 km.

UM-UKCA was run with the Chemistry of the Stratosphere and Troposphere (CheST) scheme, combining previous tropospheric (O'Connor et al., 2014) and stratospheric (Morgenstern et al., 2009) chemical schemes as used by Banerjee et al. (2014). The scheme includes 83 advected chemical tracers and 310 photochemical reactions, describing the O_x, HO_x and NO_x chemical cycles and the oxidation of CO, methane, ethane, propane and isoprene (Archibald et al., 2010, 2011).

Reaction rate coefficients were based on recommended values from the International Union of Pure and Applied Chemistry (IUPAC) Subcommittee for Gas Kinetic Data Evaluation (http://iupac.pole-ether.fr, last access: 18 May 2018), the JPL-NASA Evaluation of Chemical Kinetics and Photochemical Data for Use in Atmospheric Studies (Burkholder et al., 2015) and the Master Chemical Mechanism, MCM v3.2 (Jenkin et al., 2015), via the website: http://mcm.leeds.ac.uk/MCM (last access: 18 May 2018).

Surface emissions for the years 2000–2005 of nine trace gas species (NO_x, methane, CO, formaldehyde, ethane, propane, acetone, acetaldehyde and isoprene) were included based on Banerjee et al. (2014) as well as multilevel aircraft emissions for NO_x. Isoprene emissions were based on the MEGAN emission model (Guenther et al., 2006). The aerosol scheme also included emissions of organic carbon (OC, from both fossil fuels and biofuels), black carbon (BC,

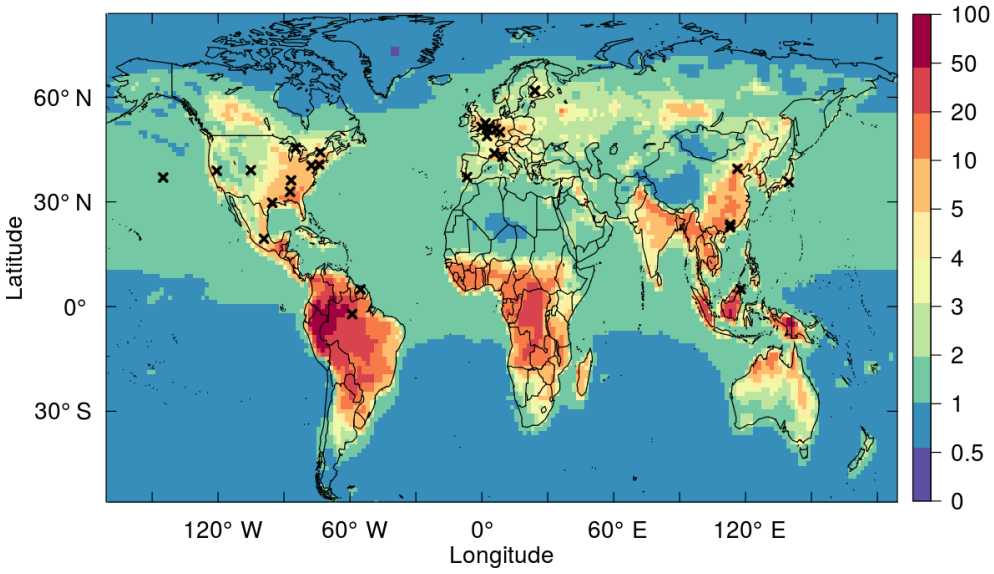


Figure 1. Annual mean of the total OH reactivity (in s^{-1}) calculated in the base run at the surface. Crosses indicate sites of field campaigns with which the model is compared.

also from both fossil fuels and biofuels), monoterpenes, SO_2, dimethyl sulfide and biogenic methanol.

The model runs used in this work are described in Table 1. They comprise a base run, discussed in detail in Sect. 3, a run with an imposed sink to account for the missing k_{OH} (X + OH run), the results of which are described in Sect. 4, and three additional experiments to explore the possible role of reactions of peroxy radicals, described in Sect. 5.2. In each run, the model was run for 5 years, with 1-year spin-up time.

A number of diagnostics widely used in models to evaluate the oxidising capacity of the troposphere, such as methane lifetime with respect to tropospheric loss via reaction with OH (τ_{CH_4}), OH lifetime (τ_{OH}) and tropospheric ozone burden, were calculated for each model scenario. τ_{CH_4} was calculated in accordance with Lawrence et al. (2001), with the troposphere defined as the domain below 250 hPa. This is also consistent with the convention used in the Atmospheric Chemistry and Climate Model Intercomparison Project (ACCMIP) (Naik et al., 2013; Voulgarakis et al., 2013). The same definition of the troposphere was used here in the calculation of tropospheric reaction fluxes and τ_{OH}. For the calculation of the tropospheric ozone burden, the troposphere was defined as the domain in which the ozone mixing ratio was below 150 ppbv (or nmol mol^{-1}), in accordance with previous studies and model intercomparisons (Ehhalt et al., 2001; Stevenson et al., 2006; Young et al., 2013). Species lifetimes were calculated by dividing the species burden by their removal rate.

3 Comparison of modelled k_{OH} and known OH sinks with observations

The modelled k_{OH} at the surface, obtained from the base run using the standard CheST scheme, is shown in Fig. 1. The total OH reactivity is lowest over oceans and remote deserts ($< 1\ s^{-1}$), highest over tropical forests ($> 10\ s^{-1}$) and somewhere between these values in urban-influenced areas. This global distribution and magnitude of k_{OH} are in reasonably good agreement with those calculated in previous modelling studies (Lelieveld et al., 2016; Safieddine et al., 2017). For reference, the modelled abundances of OH, HO_2 and RO_2 radicals in the base run are shown in Figs. S1–S3 in the Supplement.

As described in Sect. 1, many measurements of k_{OH} have been taken over the last two decades, with an exhaustive summary presented in a recent review (Yang et al., 2016). Only measurements of k_{OH} and its speciation taken over reasonably long timescales ($\geq$ 1 week) and covering the full diurnal variation of k_{OH} and of the OH sinks were considered in this work, in order to minimise biases due to day-to-day variability and to obtain a meaningful comparison with the model. A small number of field campaigns measured only the total k_{OH} and not the abundance of the individual sinks, therefore precluding the quantification of the missing reactivity or any further analysis on the speciation of k_{OH} (Michoud et al., 2015; Ren et al., 2005; Sinha et al., 2008, 2012). For these reasons, 28 field measurements of the total k_{OH} and of the individual OH sinks were used in the analysis described in this work; these are summarised in Table 2, where the values of the total k_{OH} and of the missing reactivity are reported, averaged over the whole duration of each campaign. These

observations took place in a variety of environments, the vast majority of which were situated in the Northern Hemisphere (as shown in Fig. 1). Measurement sites can be grouped into suburban (7 measurements), urban (9 measurements) and remote areas (12 measurements).

Observed k_{OH} is compared to that simulated by UM-UKCA for the same longitude, latitude and month in Fig. 2 (and in Fig. S4 in the Supplement as a scatter plot). The total observed k_{OH} in Fig. 2 is made up of contributions from the measured OH sinks, modelled intermediates (only available for some of the field campaigns presented here) and reactivity that is unaccounted for by known OH sinks, i.e. the missing reactivity. The total modelled reactivity is expected to be in good agreement with that arising from measured sinks, but this was only the case (to within $\sim 20\,\%$) in 12 out of 28 cases. Of the remaining 16 campaigns, the model underestimated the reactivity from measured sinks in 9 cases and overestimated it in 7. It is therefore important to ascertain that the modelled OH reactivity is indeed the result of the same sinks observed in the field. For this purpose, individual reactivities measured in each campaign provide a large amount of information that can be used to establish how well the model captures the speciation of k_{OH}. This is shown in Fig. 3, where the modelled reactivities from the known OH sinks are plotted against those measured in the field, and in Fig. S5 in the Supplement.

Figures 3 and S5 provide a useful guide on the magnitude of the contributions of different OH sinks to the total k_{OH}. The main contributors to k_{OH}, with reactivities ranging between 1 and $10\,s^{-1}$, are isoprene in forested environments and NO_x, CO, formaldehyde and non-methane hydrocarbons (NMHCs, indicating primarily alkanes and alkenes) in urban environments. At the other end of the spectrum, species such as methane, ozone and hydrogen only give rise to small contributions ($< 1\,s^{-1}$) to the total k_{OH}.

Overall more than half (53 %) of the reactivities calculated from modelled sinks agree with observations within a factor of 2 and the vast majority (88 %) within a factor of 10. The main source of discrepancy between modelled and observed individual reactivities are differences in the number densities of the OH sinks ($[X_i]$ in Eq. 1) and not the temperature-dependent rate constants, as temperature differences between the model and the measurements only have a minor effect on the rate constants used to calculate the reactivities. The abundance of each individual OH sink species is determined by the balance between its sources (e.g. emissions) and sinks (largely, reaction with OH). It is, however, difficult to establish whether the differences between observed and modelled OH sinks arise from misrepresenting emissions or abundances of the hydroxyl radical itself without comparing modelled and observed [OH], and measurements of the OH concentrations are only available for a small subset of the campaigns considered here. A correlation plot of modelled against observed [OH] is given in the Supplement (Fig. S6) for those campaigns that measured OH as well as the total reactivity and the individual OH sinks. At a number of sites in remote environments (BEARPEX09, CABINEX, OP3 and SOAS) the model overestimated OH by up to a factor of 6. This was attributed to the model overrepresenting NO_x in all these cases, leading to enhanced ozone abundances compared to the observations. This led to additional primary OH (from Reaction R1) in the model as well as secondary OH from $HO_2 + NO$. Overestimated OH in the model accounted for modelled isoprene concentrations lower than the measurements in a couple of cases (BEARPEX09 and CABINEX). However, in the case of the OP3 campaign, some of the modelled OH sinks were actually higher than the observations, in spite of the overestimated OH. This unexpected behaviour was attributed to the difference between the emission rates in the field and those used in the model. Emission rates of many biogenic VOCs are known to increase with temperature following an exponential curve (Di Carlo et al., 2004; Hansen et al., 2014). Upon closer inspection, the temperature at the measurement site in Borneo during the OP3 campaign was on average 5 K lower than in the model (295 K vs. 300 K). Extrapolating the isoprene emission rates from the model to the temperature observed at the measurement site resulted in a value that was half the emission rate at the temperature in the model, indicating that in this case overestimated concentrations of modelled biogenic VOCs are likely the result of the emissions rates used in the model.

The speciation of the total OH reactivity shown in Fig. 3 allows us to investigate the reasons for the discrepancy between some of the modelled k_{OH} and observations highlighted in Fig. 2. For instance, the disagreement between modelled and observed k_{OH} in some urban environments (notably Mexico City; wintertime New York; Houston; and Yufa, Beijing) is largely attributable to the underrepresentation of NMHCs in the model. This can be accounted for in terms of species lumping. As with many state-of-the-art models, instead of adding numerous hydrocarbons to the emission and chemistry schemes, the heavier alkanes and alkenes were lumped into the emission fields of ethane and propane, and weighted by carbon number. We can see that lumping serves as a reasonable approximation for the representation of the abundance of some carbon-containing species (such as CO and formaldehyde, the ultimate products of hydrocarbon oxidation, which are in reasonable agreement with observations as shown in Fig. 3 and also in Fig. S7 in the Supplement for CO). However, lumping introduces an additional complication when the OH reactivity of NMHCs is calculated. As the reactivity is defined as the product of the rate constant for the reaction of the NMHCs with OH and the number density of the NMHCs, and as the rate constants for the reaction of OH with ethane and propane are 1–2 orders of magnitude smaller than those of OH with higher alkanes ($C \geq 4$) and alkenes ($C \geq 2$), lumping leads to an underestimate of the same magnitude in the reactivity of the NMHCs.

Figure 3 also offers an explanation for the instances in which the model significantly overpredicted k_{OH}. For exam-

Table 2. Total observed OH reactivity and missing reactivity from field campaigns. These values represent averages over the whole duration of each campaign. Measurement sites are grouped into three categories (suburban, urban and remote environments respectively).

	Location (campaign)	Total observed k_{OH} s^{-1} [a]	Missing k_{OH} s^{-1} [b]	Missing k_{OH} after the inclusion of model intermediates s^{-1} [c]	k_{OH} from UKCA base run s^{-1}	Reference
Suburban	Whiteface Mountain, USA (PMTACS-NY2002)	5.40	0.02		7.1	Ren et al. (2006b)
	Weybourne, UK (TORCH-2)	4.6	2.0	1.3	7.4	Lee et al. (2009)
	Yufa, China (CAREBeijing-2006)	19.7	2.2		10.5	Lu et al. (2010)
	Backgarden, China (PRIDE-PRD)	31.4	15.7	6.3	16.2	Lou et al. (2010)
	Jülich, Germany (HOx Comp)	8.6	3.2	2.5	7.1	Elshorbany et al. (2012)
	Heshan, China	30.6	9.8	5.3	5.4	Yang et al. (2017)
	Ersa, Corsica (CARBOSOR-ChArMeX)	5.6	2.3		5.2	Zannoni et al. (2017)
Urban	Nashville, USA (SOS)	11.0	3.8		14.8	Kovacs et al. (2003)
	New York, USA (PMTACS-NY2001)	18.8	0.7		15.4	Ren et al. (2003a, b)
	New York, USA (PMTACS-NY2004)	25.1	4.0		9.1	Ren et al. (2006a)
	Mexico City, Mexico (MCMA-2003)	47.5	14.3		5.2	Shirley et al. (2006)
	Houston, USA (TexAQS)	9.4	0.4		8.7	Mao et al. (2010)
	Houston, USA (TRAMP2006)	12.24	0.03		8.9	Mao et al. (2010)
	Paris, France (MEGAPOLI)	40.3	22.8		4.6	Dolgorouky et al. (2012)
	Lille, France	7.4	0		4.8	Hansen et al. (2015)
	London, UK (ClearfLo)	18.1	5.9	2.7[d]	6.0	Whalley et al. (2016)
Remote	Michigan, USA (Prophet2000)	7.8	2.6		4.8	Di Carlo et al. (2004)
	Hyytiälä, Finland (BFORM)	8.6	3.9		6.3	Sinha et al. (2010)
	Hyytiälä, Finland (HUMPPA-COPEC2010)	11.5	8.9		6.6	Nölscher et al. (2012)
	Rocky Mountains, USA (BEACHON-SRM08)	6.7	2.1		3.5	Nakashima et al. (2014)
	Michigan, USA (CABINEX)	11.6	6.3		4.8	Hansen et al. (2014)
	Amazon, Brazil (ATTO) dry season	49.6	35.8		35.8	Nölscher et al. (2016)
	Amazon, Brazil (ATTO) wet season	8.3	3.9		43.4	Nölscher et al. (2016)
	Haute Provence, France (CANOPEE)	17.9	1.1		5.6	Zannoni et al. (2016)
	Borneo, Malaysia (OP3)	15.3	10.2	5.8	15.3	Edwards et al. (2013)
	Alabama, USA (SOAS)	19.4	4.9	3.6	21.1	Kaiser et al. (2016)
	California, USA (BEARPEX09)	17.3	7.1	3.5	6.9	Mao et al. (2012)
	North Pacific (INTEX-B)	4.0	2.2		1.1	Mao et al. (2009)

[a] These values are the mean of the total k_{OH} measured over the whole duration of each field campaign.
[b] Missing reactivity calculated as the difference between the total k_{OH} and the sum of the individual reactivities arising *exclusively* from measured OH sinks.
[c] Missing reactivity calculated as the difference between the total k_{OH} and the sum of the individual reactivities arising from *both* measured OH sinks and intermediates modelled in the particular studies referenced.
[d] The addition of unidentified compounds observed by two-dimensional gas chromatography with flame ionization detection (GC × GC-FID) reduced the missing reactivity further to only $\sim 1.1\ s^{-1}$.

ple, the abundance of isoprene measured during the wet season of the ATTO campaign in the Amazon ($\sim 1 \pm 0.1$ ppbv, or nmol mol^{-1}, in March 2013) was more than an order of magnitude lower than that predicted by the model for the same time of the year (~ 14.6 ppbv). As discussed above, this might arise from either overestimated isoprene emissions or from underestimated OH abundances in the model. As OH concentrations were not measured during the ATTO campaign, a direct comparison of modelled and observed [OH] is not possible. However, [OH] measurements from campaigns carried out in neighbouring parts of the Amazon (Liu et al., 2016) and in the Suriname rainforest (Martinez et al., 2010) might help address this point. Indeed the model underestimates [OH] by almost a factor of 4 on average in both cases, although it is worth noting that [OH] measurements from Liu et al. (2016) only cover ~ 7 h on a single day, whilst the GABRIEL campaign in Suriname consisted of airborne measurements, and only the OH data for the boundary layer were considered for comparison with the model. It may also be indicative of underrepresented [OH] in model that the abundance of other short-lived OH sinks in the ATTO campaign is also overestimated by the model; notably, the observed concentration of monoterpenes (reported to be below the detection limit of the proton transfer reaction mass spectrometer used by Nölscher et al. (2016), and here approximated to 0.01 ppbv) was much lower than in the model (2.2 ppbv). Underrepresented OH in the model might arise from underestimating the secondary OH originating from the oxidation of large organics (e.g. isoprene and monoterpenes, as described in Archibald et al., 2010). In this specific instance the model also underestimated the concentration of NO (34 pptv, or pmol mol^{-1}, vs. the observed $\sim 1 \pm 0.05$ ppbv), which might have limited the production of secondary OH via the reaction of HO_2 with NO relative to observations, in contrast with other remote environments in which OH was overestimated.

The methane lifetime with respect to tropospheric loss via reaction with OH, τ_{CH_4}, for the base run was 8.75 years, which is within 1σ of the ACCMIP multimodel mean for the year 2000 (9.7 ± 1.5 years). τ_{CH_4} from the base run is also in good agreement with the value of 8.5 years reported by Lelieveld et al. (2016). Notably the model used by these authors exhibited some differences from the one used in the current work: Lelieveld et al. (2016) used emissions for the year 2010, defined the tropopause via their own diagnostic

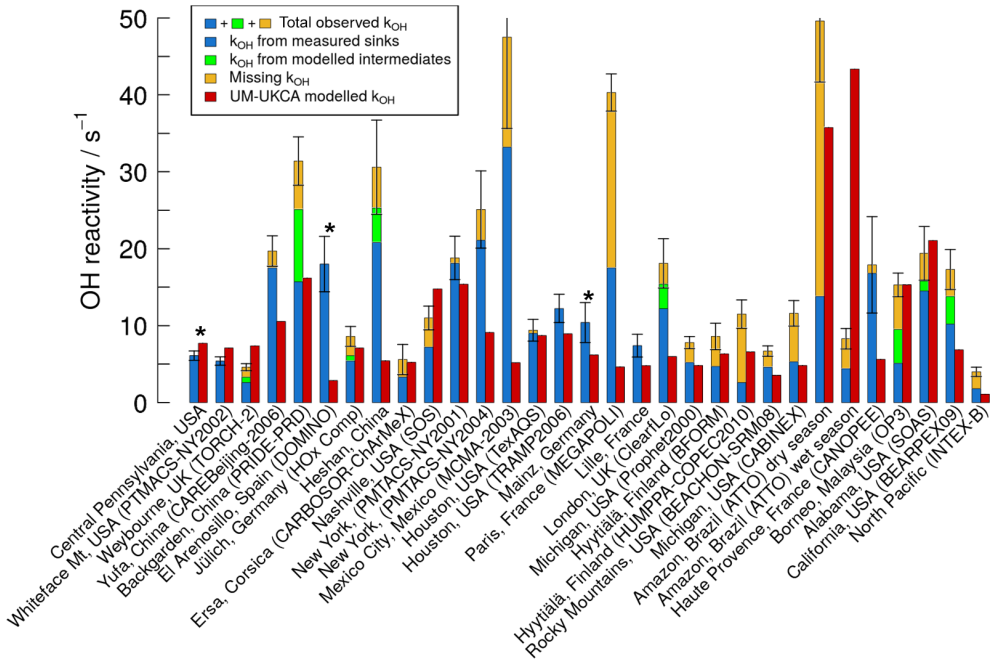


Figure 2. Comparison of the average observed k_{OH} with modelled k_{OH}. The total k_{OH} measured in each field campaign is represented by the sum of the blue, green and yellow bars. Blue bars represent the OH reactivity accounted for by measured OH sinks, green bars represent the OH reactivity accounted for by modelled reaction intermediates (only available for some of the studies presented here) and yellow bars represent the OH reactivity which is unaccounted for (i.e. the missing reactivity). Red bars represent the total OH reactivity calculated from the modelled data in the UM-UKCA base run. Error bars represent the uncertainties (at the 1σ level) in the total k_{OH} measurement. Asterisks indicate campaigns in which only the total k_{OH} was measured, without detection of the individual OH sinks. In these cases the blue bar represents the total observed k_{OH}. A version of this plot detailing the speciation of both observed and modelled reactivity is given in the Supplement in Fig. S5.

and employed an extensive chemistry scheme consisting of 1630 reactions. Notwithstanding these differences, the values for τ_{CH_4} from the two studies are in very good agreement. In the base run, the average lifetime of the OH radical, τ_{OH}, was 1.18 s for the whole troposphere, 0.57 s within the boundary layer and 0.45 s at the surface, as summarised in Table 4.

4 Modelling the missing reactivity: addition of sink X

Figure 3 highlights that whilst the model represents many of the individual components of OH reactivity within at least an order of magnitude (and often within a factor of 2) of observations, the model underrepresents total k_{OH} in the majority of the cases (Fig. 2). There are a number of ways to account for this missing reactivity in the model. For example, additional species (such as more reactive NMHCs or more reactive reaction intermediates) and their chemistry could be included in the model. However, observations indicate that this approach would still leave outstanding missing reactivity (Edwards et al., 2013; Elshorbany et al., 2012; Kaiser et al., 2016; Kovacs et al., 2003; Lee et al., 2009; Lou et al., 2010; Mao et al., 2012; Mogensen et al., 2011; Yang et al., 2017). In this work, we have taken a different, simpler approach. A new species representing a direct sink of OH was added to the model and its atmospheric implications were assessed. Emissions of the unspecified OH sink, species X, were introduced in the model simulations along with the reaction:

$$X + OH \rightarrow \text{products}, \quad \text{(R3)}$$

with a temperature-independent bimolecular rate constant, $k_3 = 1 \times 10^{-10}\,\text{cm}^3\,\text{molecules}^{-1}\,\text{s}^{-1}$, set to represent reactions with a very reactive compound (i.e. OH + reactive VOCs). Crucially, the global and seasonal abundance of X was underpinned by field observations of missing k_{OH}. This section discusses the implementation of this scheme in the model and its effects.

4.1 Generating a global field of missing reactivity

To generate a surface field for the missing reactivity, multiple linear regression was applied. This method consisted of fitting the missing reactivity from observations to the corresponding model grid box emissions of VOCs, NO_x and aerosol precursors at the individual observation sites where the OH reactivity was measured (described in Sect. 2). This resulted in a time-varying spatial field for the missing reactivity based on the predictors (emission fields) listed in

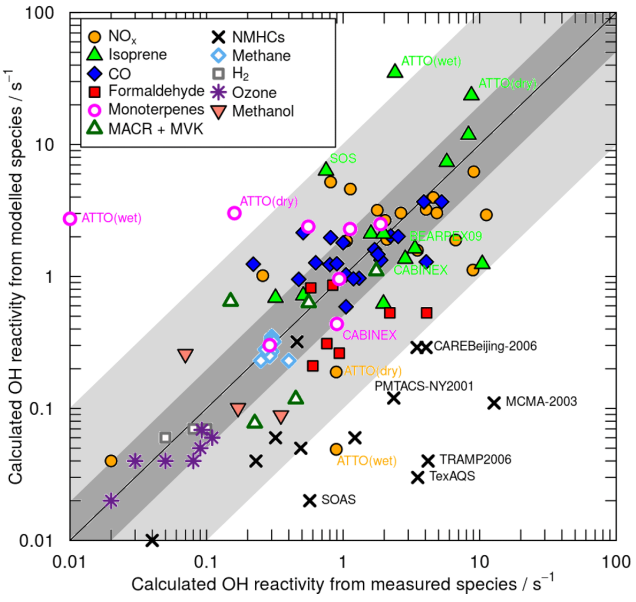


Figure 3. Scatter plot of modelled OH reactivity arising from known OH sinks against measurements. Also shown is the 1 : 1 line (solid black line) as well as the factor-of-2 and factor-of-10 deviations from it (dark-grey and light-grey areas respectively). Specific data points that are discussed in the text are labelled with the name of the field campaign in which those particular measurements were taken.

Table 3. Outcome of the multiple linear regression (MLR). The predictors are sorted by increasing p value.

Predictor	Coefficient/10^{12} kg^{-1} m^2
OC biofuel emissions	4.41
BC biofuel emissions	−12.97
Acetone emissions	0.78
CO emissions	−0.02
OC fossil fuel emissions	−0.67
BC fossil fuel emissions	1.25
Monoterpene emissions	0.04
NO_x emissions	−0.02
Isoprene emissions	−0.02
Methane emissions	0.01
Acetaldehyde emissions	−1.18
Formaldehyde emissions	1.20
Biogenic methanol emissions	−0.02
Ethane emissions	−0.22
Propane emissions	0.76

Table 3. Correlation of the missing k_{OH} with some of the emitted species would be expected, both if the missing sink was an oxidation intermediate (in which case it would correlate with its precursors) and if it was a primary emission (in which case it could be expected to correlate to other primary emitted VOCs such as anthropogenic or biogenic VOCs). This is also supported by observations. For instance, measurements taken during the INTEX-B campaign (Mao et al., 2009) found that the missing reactivity correlated with formaldehyde concentrations; the authors concluded that this indicated that the missing reactivity potentially arose from VOCs that formed formaldehyde upon oxidation. Similarly, measurements taken in a forest in Michigan during the CABINEX campaign showed good correlation between the missing reactivity and both isoprene and its oxidation products (methyl vinyl ketone, MVK, and methacrolein, MACR) when the missing reactivity was highest (Hansen et al., 2014).

The results of the multiple linear regression using all 15 predictors in Table 3 are shown in Fig. 4; the R^2 value for the fit was 0.75. The strongest predictors of the missing reactivity were the emissions of organic carbon from biofuels (OC biofuel), black carbon from biofuels (BC biofuel), acetone and CO. Whilst these might indicate both an anthropogenic and a biogenic component of the missing reactivity, none of the predictors had a p value ≤ 0.05 (with OC biofuel coming close with $p = 0.067$), perhaps as a result of the small sample size available. The coefficients from the multiple linear regression are shown in Table 3. The fact that the strongest predictors were the emissions for aerosol tracers not included in the model gaseous chemistry might also indicate potential contributions to the total k_{OH} from condensed-phase particles. However, the role of particulate matter in OH loss is very poorly characterised, as highlighted in the recent review by Yang et al. (2016).

To establish the robustness of the outcome of the multiple linear regression routine, the analysis was repeated using different subsets of predictors. Unsurprisingly, the iterations using larger numbers of predictors returned better error statistics (R^2 values, normalised mean biases, etc.). The inclusion of the bottom three predictors in Table 3 (biogenic methanol, ethane and propane emissions) led to only marginal improvements in the quality of the fit (e.g. increases in $R^2 < 0.1$ %) in all cases. On the other hand, the top four entries in Table 3 were the strongest predictors in all iterations that included them, and their exclusion from the fitting routine affected the quality of the fit significantly (e.g. decreases in $R^2 > 10$ %). For the purpose of this work, the outcome of the multiple linear regression with all 15 predictors was used.

The multiple linear regression resulted in an expression of missing reactivity at the surface, varying with longitude, latitude and time. Figure 5 shows global seasonal averages of the modelled missing reactivity at the surface in boreal winter (DJF) and summer (JJA). The multiple linear regression captured some of the seasonality of the missing reactivity over forested regions at midlatitudes: this behaviour is consistent with the temperature dependence of the missing reactivity observed in a number of field campaigns in forested areas (as described in Sect. 1). In addition, a number of urban areas are also distinguishable as regions of high missing reactivity.

Overall, the modelled missing reactivity obtained from the multiple linear regression had values other than zero in 23 %

Table 4. Values of the OH and methane lifetimes in the model runs described in this work. Numbers in brackets indicate the percentage change with respect to the base run.

	Base run	X+ OH run	CH_3O_2 + OH run 1	CH_3O_2 + OH run 2	CH_3O_2 + OH run 3
τ_{OH} surface/s	0.455	0.447 (−1.8 %)	0.442 (−2.7 %)	0.442 (−2.7 %)	0.442 (−2.7 %)
τ_{OH} boundary layer/s	0.574	0.557 (−3.2 %)	0.558 (−2.8 %)	0.558 (−2.8 %)	0.558 (−2.8 %)
τ_{OH} troposphere/s	1.18	1.16 (−1.5 %)	1.15 (−2.5 %)	1.15 (−2.5 %)	1.15 (−2.5 %)
τ_{CH_4}/years	8.75	8.95 (+2.3 %)	8.92 (+2.0 %)	8.97 (+2.5 %)	9.01 (+3.0 %)

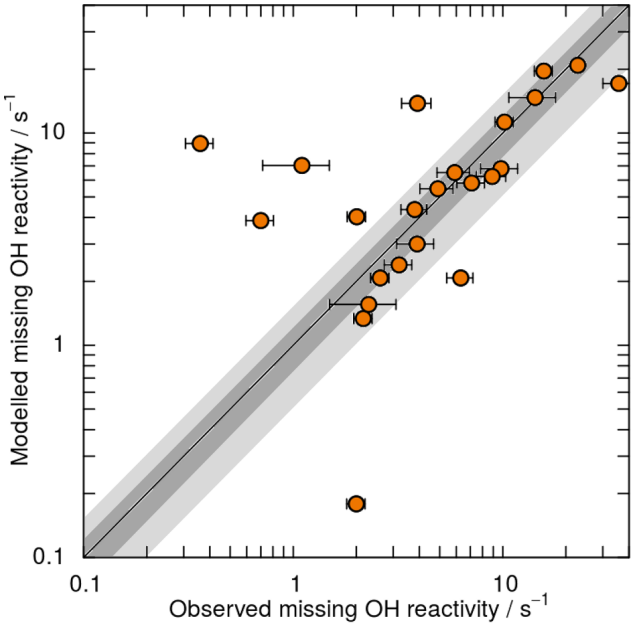


Figure 4. Scatter plot of missing OH reactivity modelled by multiple linear regression against observed missing OH reactivity (as reported in Table 2). Each point represents one observation site. The error bars mirror the uncertainties (at the 1σ level) from each individual measurement of the total k_{OH}. Also shown is the 1 : 1 line (solid line), as well as the 20 and 50 % deviations from it (dark-grey and light-grey areas respectively). The R^2 value from the multiple linear regression was 0.75.

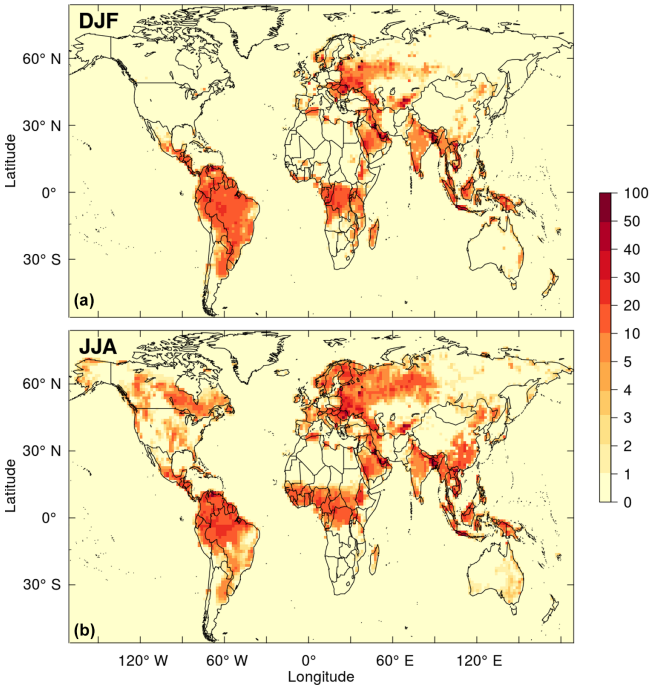


Figure 5. Global distribution of the simulated missing OH reactivity (in s^{-1}) in boreal winter (DJF, **a**) and boreal summer (JJA, **b**).

of the surface grid cells in DJF and in 32 % of the grid cells in JJA. Of all the non-zero values plotted in Fig. 5, 57 % are below 1 s^{-1}, 77 % are below 5 s^{-1}, 87 % are below 10 s^{-1} and 99.8 % are below 50 s^{-1}. Only a very small number of grid cells have modelled missing reactivities in the range 50–100 s^{-1} (12 grid cells in DJF and 15 in JJA). These regions correspond to areas of high anthropogenic emissions that resulted in large contributions of the strongest predictors (OC and BC biofuels) to the calculated missing reactivity.

In order to establish the effects of the additional sink on tropospheric oxidation chemistry it is necessary to emit species X in the model and let it interact with OH via Reaction (R3). However, the conversion of the global missing reactivity derived from the multiple linear regression into an emission field is not straightforward. Initially, the emission rate of X is calculated as equal to the rate of removal of X within the turbulent boundary layer for each surface grid cell, according to Eq. (2):

$$\text{Emission rate of X / kg m}^{-2}\,\text{s}^{-1} = k_3[\text{X}][\text{OH}] \times \frac{h\ M_r}{N_\text{A}} \times 10^3, \quad (2)$$

where k_3 is the rate constant for Reaction (R3) (in cm^3 molecules^{-1} s^{-1}), [X] and [OH] are the number densities of X and OH respectively (in units of molecules cm^{-3}), h is the height of the turbulent boundary layer (in metres), M_r is the molar mass of species X (arbitrarily assigned a value of 30 g mol^{-1}) and N_A is Avogadro's number (in molecules mol^{-1}). The term k_3[X] corresponds to the missing reactivity from the multiple linear regression, whilst the values of [OH] are taken from the base run. The model was run for 1 year with these emissions of X. Then the OH reactivity arising from the newly emitted species X was calculated for

the model run (as k_3[X]) and compared with the missing reactivity obtained from the multiple linear regression. It was found that the OH reactivity arising from species X in this initial model run was significantly higher than the missing reactivity determined via multiple linear regression (as shown in Fig. 6b). This overestimate was attributed to the fact that the OH field from the base run used in Eq. (2) is itself an overestimate of the OH field from a scenario where an additional sink (species X) is introduced. A routine was therefore developed, in which the initial emission field of species X was iteratively optimised in a series of model runs until the OH reactivity from species X in the model matched the missing reactivity determined via multiple linear regression within the tolerances specified in Fig. 6a. The procedure used is summarised in Fig. 6. As the missing reactivity from the multiple linear regression was underpinned by observations, this routine ensured that the additional sink emitted in the model would still account for the observed missing reactivity.

4.2 Effects of introducing sink X

The chemistry used for sink X does not allow any secondary OH formation following the initial oxidation of X in Reaction (R3). This is unrealistic, as the oxidation of the vast majority of trace species leads to some degree of secondary OH production; however, with so little information available on the identity of species X, the system was too poorly constrained to even attempt an educated guess on the OH recycling probability of the products of Reaction (R3). Therefore the effects of introducing sink X in the model, discussed at length in this section, can be seen as a "worst case" scenario, one in which no OH is regenerated following Reaction (R3) and in which OH is removed from regions of high emissions of X. This may be the case for reactions of OH on aerosol surfaces.

OH abundances are reduced following inclusion of Reaction (R3) in the chemistry scheme, as a result of both direct removal of OH via Reaction (R3) and less efficient production of secondary OH (as highlighted in the fluxes reported in the Supplement). As shown in Fig. 7, the most OH-depleted areas at the surface include Scandinavia, eastern Europe and the coastlines of the Persian Gulf, Venezuela and Java. Peak OH reductions in these regions are of the order of 5–6 $\times 10^6$ molecules cm^{-3}. In these regions as much as 90 % of the mean annual [OH] is removed, but it must be stressed that secondary OH production from the products of Reaction (R3) would mitigate these effects. Interestingly some of the regions affected by the highest emissions of X (i.e. the Amazon region and central Africa) only exhibit relatively small decreases in OH concentrations of $\sim$ 20 %; as these areas are rich in OH sinks, the introduction of an additional sink does not affect the OH budget significantly. OH depletion is most pronounced at the surface and in the boundary layer in the Northern Hemisphere (also in Fig. 7), which is consistent with the vertical distribution of the additional OH reactivity brought about by species X shown in Fig. 8. Mean tropospheric OH decreased by 1.6 %, whilst mean OH abundances in the boundary layer and at the surface were reduced by 5.6 and 8.1 % respectively. Seasonal changes in OH abundances, both in absolute and relative terms, are shown in Figs. S8 and S9 in the Supplement. These show significant relative reductions in the mean boreal winter OH in the Northern Hemisphere (> 60 %), which are, however, very small in absolute terms (< 5 $\times 10^4$ molecules cm^{-3}). Changes in HO_2 mainly mirror those in OH, albeit with a somewhat smaller relative magnitude (see Fig. S10 in the Supplement).

τ_{CH_4} for the model run including Reaction (R3) was 8.95 years ($\sim$ 2.3 % higher than the base run). τ_{OH} was reduced by approximately 2 % at the surface, by 3 % in the boundary layer and by 1.5 % in the whole troposphere (Table 4). Another metric of interest when discussing tropospheric oxidation chemistry is the OH recycling probability, r, which describes the sensitivity of the OH chemistry to perturbations (Lelieveld et al., 2002). r was calculated in accordance with Lelieveld et al. (2002, 2016), using Eq. (3):

$$r = 1 - P/G, \tag{3}$$

where P is the rate of formation of primary OH (i.e. via Reaction R1 and Reaction R2) and G is the gross OH formation rate, consisting of the sum of P and the formation rate of secondary OH, S (i.e. via any route other than Reaction R1 and Reaction R2). Using the OH formation fluxes tabulated in the Supplement (Tables S1–S3), it was found that r remained larger than 60 % in both runs, indicating that tropospheric oxidation was effectively "buffered".

The ozone burden at the surface decreased slightly by 0.9 %, but the overall tropospheric ozone burden increased by 0.3 %. This somewhat contradictory behaviour in ozone, also shown in Fig. 9, can be accounted for in terms of the changes brought about by decreases in OH in regions with different NO_x abundances. In general, OH decreases are accompanied by lower concentrations of HO_2 and peroxy radicals (RO_2); in OH-depleted, NO_x-rich regions (e.g. Europe in Fig. 9) less HO_2 and RO_2 are available to react with NO, leading to a reduction in ozone produced from NO_2 photolysis. On the other hand, in remote regions with low NO_x the lower abundance of HO_2 and RO_2 following sequestration of OH by X leads to less efficient ozone removal via the reaction of O_3 with HO_2 (and, to a lesser extent, via the reaction of HO_2 with RO_2, producing soluble alkyl hydroperoxides), which appears as a slight positive change in Fig. 9. Decreases in surface ozone in the Northern Hemisphere are also exacerbated by the absence of further chemistry following Reaction (R3). This rules out the production of X-peroxy radicals from the initial oxidation of X, which in turn would react with NO to produce NO_2, the photolysis of which would then lead to O_3 formation. However, to what degree the ozone changes shown in Fig. 9 would be mitigated by subsequent chemistry

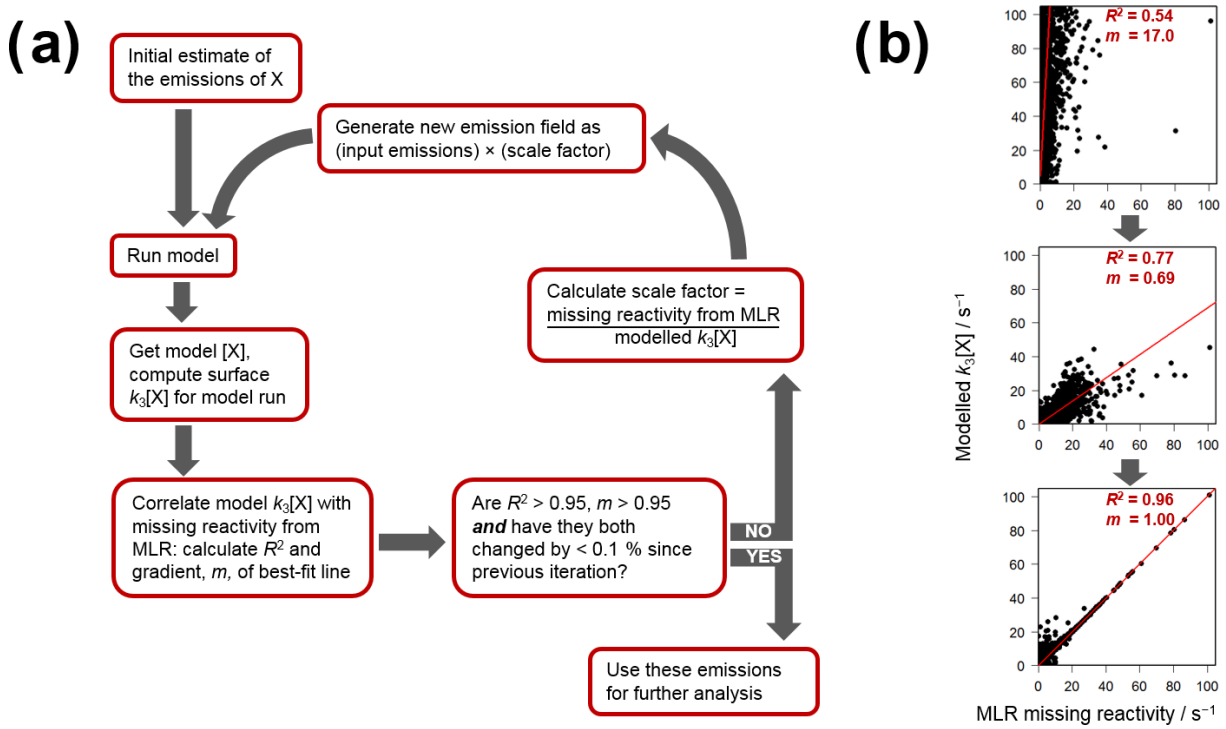


Figure 6. Implementation of the routine used to convert the global missing reactivity field obtained from multiple linear regression (MLR) into emissions of species X. Panel **(a)** illustrates the procedure as a flow chart, whilst panel **(b)** shows the correlation plots between modelled k_3[X] and the MLR missing reactivity from non-consecutive iterations. As the R^2 values and the gradients of the correlation plots converge to 1, the emissions of X in the model lead to X-reactivities identical to the missing reactivity derived by MLR.

would be highly dependent on the actual nature of the missing sink. Comparison of ozone seasonal observations from a number of remote sites with the model output (illustrated in Fig. S11 in the Supplement) shows that, whilst generally the model and the observation are in good agreement in a number of the locations shown, the inclusion of the additional OH sink X has a minimal impact on the modelled ozone at these locations.

On average, Reaction (R3) accounts for approximately 6 % of the total OH loss flux at the surface (see Table S3 in the Supplement.); in some particular regions, such as the Amazon rainforest, this contribution increases to up to 20 %, whilst in areas of eastern Europe it increases up to 50 % (see Fig. S12 in the Supplement). As a result, reactions of OH with other sinks (e.g. methane) become less efficient and the lifetime of such species increases: the lifetime of isoprene, a major tropospheric OH sink, increases by 17 % from 2.36 to 2.76 h. This is reflected in the reduced flux through its reaction with OH in the regions of high X reactivity (Tables S1–S3). As a result of its longer lifetime, isoprene is transported to higher altitudes than in the base run, as the flux through its reaction with OH increases above the boundary layer.

Whilst the work described in this section can be considered a worst-case scenario due to the absence of OH recycling following Reaction (R3), it is important to observe that the impacts on the wider atmosphere are relatively minor. Reconciling the observations of missing OH reactivity in our model in a worst-case scenario (for OH) has little impact on the global oxidising capacity. We report a small increase in methane lifetime, and an overall minor decrease in surface ozone; however, the actual extent of these changes in the real atmosphere is likely to be mitigated to some degree by OH recycling following the initial oxidation of the missing sink.

5 Effects of $RO_2 + OH$ chemistry

The previous section focused on simulating the observed missing reactivity by introducing an additional sink in the form of species X. Based on structural-reactivity arguments, Archibald et al. (2009) postulated that there could be a reaction between peroxy radicals (RO_2) and OH which could act as a sink for OH and, depending on the mechanism, a potential source of oxygenated VOCs. A lack of any experimental data hampered estimations of the rate constant for the reaction. However, recent laboratory studies have confirmed that peroxy radicals do indeed react with OH and, subsequently, the kinetics of the simplest $RO_2 + OH$ reactions have been characterised (Fittschen et al., 2014). The potential impact of RO_2 species as OH sinks and their contribution to the total OH reactivity have not been investigated to date.

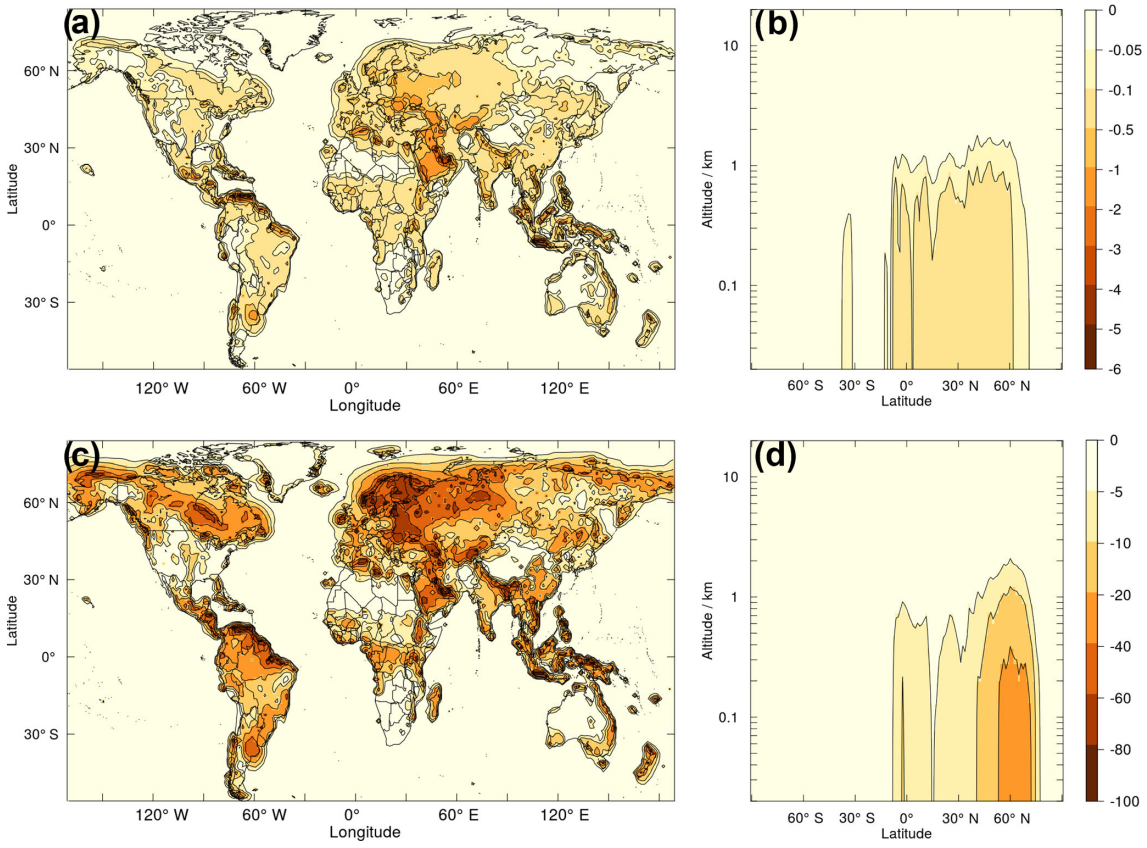


Figure 7. Annual mean change in OH concentration following inclusion of Reaction (R3): absolute change in 10^6 molecules cm^{-3} **(a)** at the surface and **(b)** as a zonal mean, and relative percentage change **(c)** at the surface and **(d)** as a zonal mean.

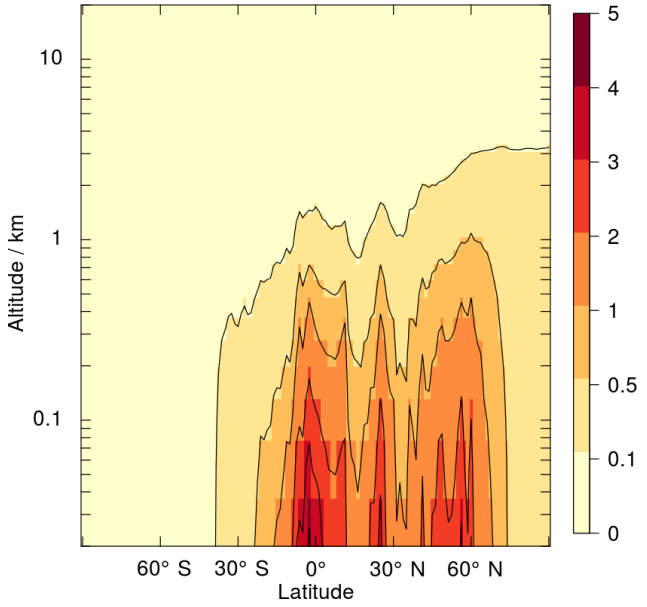


Figure 8. Annual zonal mean of the OH reactivity (in s^{-1}) arising from sink X.

5.1 Overall contribution of modelled RO_2 to k_{OH}

The UM-UKCA base model described in Sect. 2 includes the formation and reactions of a number of peroxy radicals. These include not only those originating from the oxidation of the simplest alkanes (methane, ethane and propane) and carbonyl compounds (acetaldehyde, propanal, acetone), but also those formed from isoprene and its oxidation products (methacrolein and methyl vinyl ketone). This allowed the offline calculation of an additional term for k_{OH} arising from the contributions of all RO_2 radicals in the model, k'_{OH}, as shown in Eq. (4):

$$k'_{OH} = \sum_{i=1}^{n} k_{OH+RO_{2,i}} \left[RO_{2,i}\right], \quad (4)$$

where $[RO_{2,i}]$ is the concentration of peroxy radical i and $k_{OH+RO_{2,i}}$ is the rate constant of its reaction with OH. The total concentration of all RO_2 species in the base run is shown in Fig. S3 in the Supplement. Assumptions had to be made as to the individual values of $k_{OH+RO_{2,i}}$, as only the rate constants of the reactions of OH with methyl (Assaf et al., 2016, 2017b; Bossolasco et al., 2014; Yan et al., 2016), ethyl (Assaf et al., 2017a; Faragó et al., 2015), propyl (Assaf et al.,

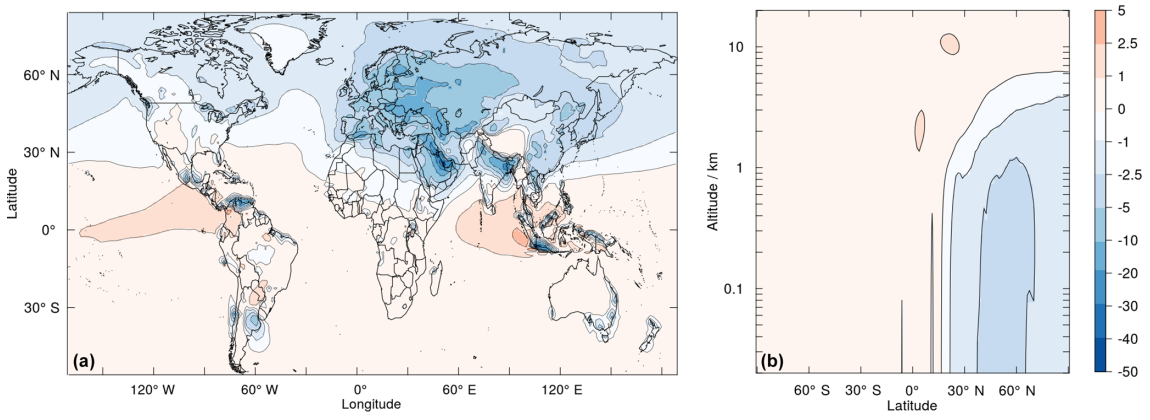


Figure 9. Annual mean percentage change in O_3 concentration at the surface **(a)** and as a zonal mean **(b)**.

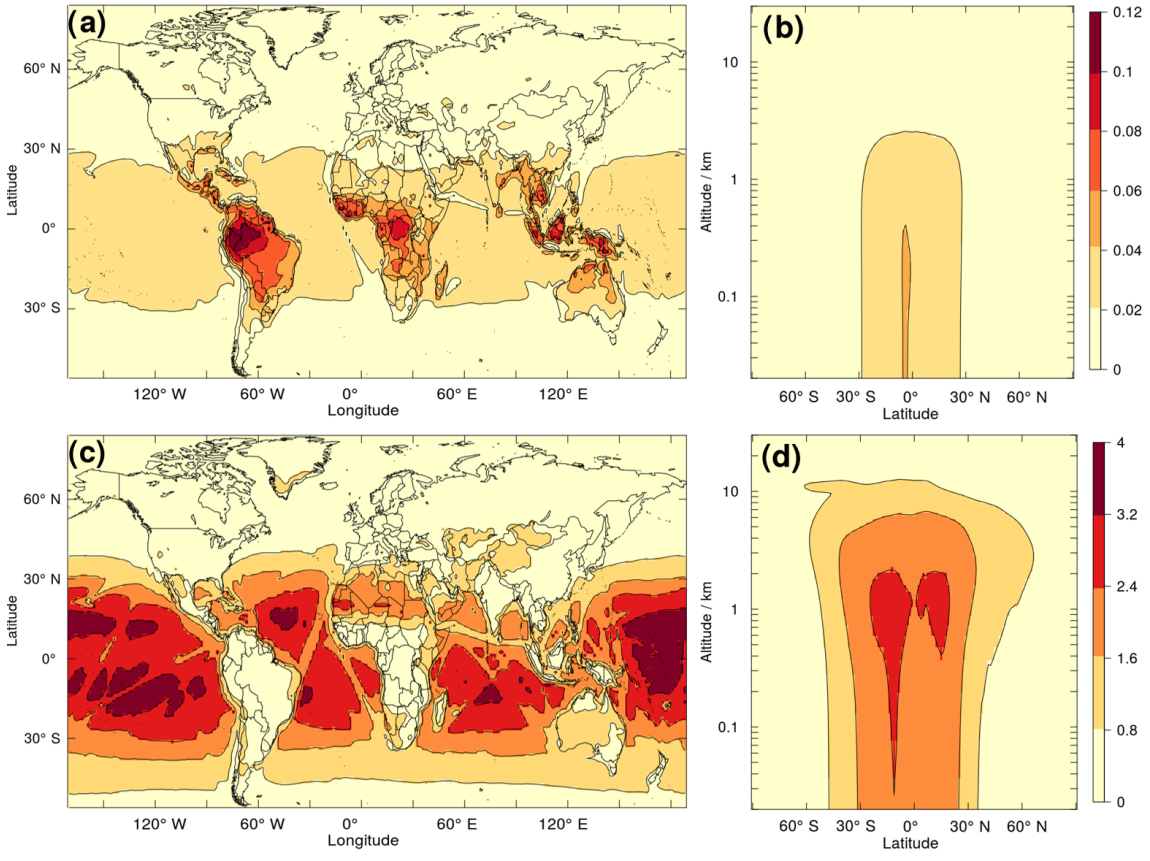


Figure 10. Changes in total k_{OH} from the inclusion of $RO_2 + OH$ reactions: **(a)** global surface change in s^{-1} and **(b)** zonal mean in s^{-1}; **(c)** percentage change at the surface and **(d)** percentage change zonal mean.

2017a) and *i*- and *n*-butyl (Assaf et al., 2017a) peroxy radicals have been measured in the laboratory to date. Reported experimental values for the rate constant of the reaction of the simplest peroxy radical, CH_3O_2, with OH disagree by more than a factor of 3. The highest value to date, reported by Bossolasco et al. (2014) (2.8×10^{-10} cm^3 molecule^{-1} s^{-1} at $T = 294$ K), has since been revised to a lower value (1.6×10^{-10} cm^3 molecule^{-1} s^{-1} at $T = 295$ K) by the same group (Assaf et al., 2016): the difference is thought to arise from complicating secondary chemistry due to the presence of electronically excited iodine atoms following the photolysis of the gaseous mixture used by Bossolasco et al. (2014). However, an even lower value has been reported by Yan et al. (2016) (8.4×10^{-11} cm^3 molecule^{-1} s^{-1} at $T = 298$ K),

and the reason for the discrepancy between this study and that by Assaf et al. (2016) is still unclear.

In general, the rate constants of these reactions exhibit no significant dependence on the size of the alkyl group on the RO_2 radical. For the purpose of this study all $k_{OH+RO_{2,i}}$ were assumed to be equal to the rate constant of the reaction of the methyl peroxy radical with OH at $T = 295\,K$ as measured by Assaf et al. (2016) and were independent of temperature. Equation (4) therefore can be rewritten as

$$k'_{OH} = k_{OH+RO_2} \sum_{i=1}^{n} [RO_{2,i}], \quad (5)$$

where $k_{OH+RO_2} = 1.6 \times 10^{-10}\,cm^3\,molecule^{-1}\,s^{-1}$.

The additional annual mean OH reactivity at the surface resulting from RO_2 chemistry is shown in Fig. 10: whilst the largest contributions in absolute terms to the total k_{OH} are found in forested tropical regions (Fig. 10a, where RO_2 radicals from isoprene dominate), these are indeed very small when compared to the total reactivity present in the same regions. In relative terms, RO_2 radicals are most significant as OH sinks over remote tropical oceans (Fig. 10c), where the majority (> 90 %) of the RO_2 contribution to k_{OH} arises from the methyl peroxy radical. This contribution extends beyond the boundary layer and into the free troposphere over tropical latitudes, as shown in Fig. 10b and d.

5.2 The CH_3O_2 + OH reaction and product branching simulations

Recent studies on the products of the reaction of the simplest peroxy radical, CH_3O_2, with OH allow extension of the work described in the previous section by investigating the impact on the total k_{OH} not only of the peroxy radical, but also of some of the reaction products. Three product channels can be envisaged for this reaction (Archibald et al., 2009):

$$CH_3O_2 + OH \rightarrow HO_2 + CH_3O, \quad (R4a)$$

$$\rightarrow H_2O + CH_2O_2, \quad (R4b)$$

$$\rightarrow O_2 + CH_3OH, \quad (R4c)$$

with branching ratios defined as

$$\alpha = k_{4a}/(k_{4a} + k_{4b} + k_{4c}), \quad (6a)$$

$$\beta = k_{4b}/(k_{4a} + k_{4b} + k_{4c}) \quad (6b)$$

$$\gamma = k_{4c}/(k_{4a} + k_{4b} + k_{4c}). \quad (6c)$$

Recent laboratory studies identified Reaction (R4a) as the major product channel, with $\alpha = 0.80 \pm 0.20$ (Assaf et al., 2017b). Reaction channel (R4b), producing the Criegee intermediate CH_2O_2, was found to be a minor contributor to the overall reaction ($\beta < 0.05$). As the set-up used in the study was not suitable for the detection of methanol (CH_3OH), the magnitude of γ could not be established. A theoretical study identified Reaction (R4c) as a potentially significant source of methanol in the remote boundary layer and modelled its impacts (Müller et al., 2016). However, this study predated the first (and, so far, only) experimental determination of the products of Reaction (R4), and also used the very high value of k_4 reported by Bossolasco et al. (2014), which has since been revised to a value almost a factor of 2 lower than the original (as discussed in Sect. 5.1).

In the current work, three simulations were run with different sets of values for α and γ (run 1: $\alpha = 1$, $\gamma = 0$; run 2: $\alpha = 0.8$, $\gamma = 0.2$; run 3: $\alpha = 0.6$, $\gamma = 0.4$) in order to establish the atmospheric implications of different product branching for Reaction (R4) over the uncertainty range of α reported by Assaf et al. (2017b).

As shown in Table 4, introduction of Reaction (R4) to the model led to shorter τ_{OH} (by approximately 3 %), regardless of the product branching. Tropospheric methane lifetime increased by as much as 3 % in run 3. HO_2 abundances increased in all runs and in particular in run 1, which exhibited HO_2 concentrations higher than the base run by as much as 12 % over remote oceans, as shown in Fig. 11. Mean tropospheric HO_2 abundances increased by 3.9 % in run 1, 2.8 % in run 2 and 1.7 % in run 3.

Regardless of the product branching of Reaction (R4), the concentration of methyl peroxy radicals at the surface decreased significantly (by as much as 30 %) over remote oceans and more moderately (by 5–10 %) over land at midlatitudes (Fig. 12). Mean tropospheric CH_3O_2 abundances decreased by 14 % in all runs, whilst mean tropospheric OH was reduced by 1.5 % in run 1, 2.1 % in run 2 and 2.7 % in run 3.

The inclusion of Reaction (R4) in the model led to a small reduction ($\sim$ 1 %) in the tropospheric ozone burden. This is mainly driven by the increase in HO_2 abundances, leading to enhanced ozone removal via $O_3 + HO_2$ over remote oceans. Ozone abundances over NO_x-rich areas were largely unchanged, as the reaction of CH_3O_2 with NO dominates over Reaction (R4) and therefore HO_2 concentrations did not deviate significantly from the base run.

The largest difference in the impact of different branching ratios for Reaction (R4) was observed for methanol concentrations, as shown in Fig. 13. In the scenario in which $\alpha = 1$ (and $\gamma = 0$), methanol concentrations decrease by as much as 40–50 % over remote oceans as Reaction (R4a) efficiently inhibits methanol production via the CH_3O_2 self-reaction. However, increasing γ increases methanol mixing ratios. When $\gamma = 0.4$ methanol abundances are enhanced by up to 300 % (relative to the base case) over remote regions. Mean tropospheric methanol decreased by 8.4 % in run 1 and increased by 35.9 and 80.2 % in runs 2 and 3 respectively.

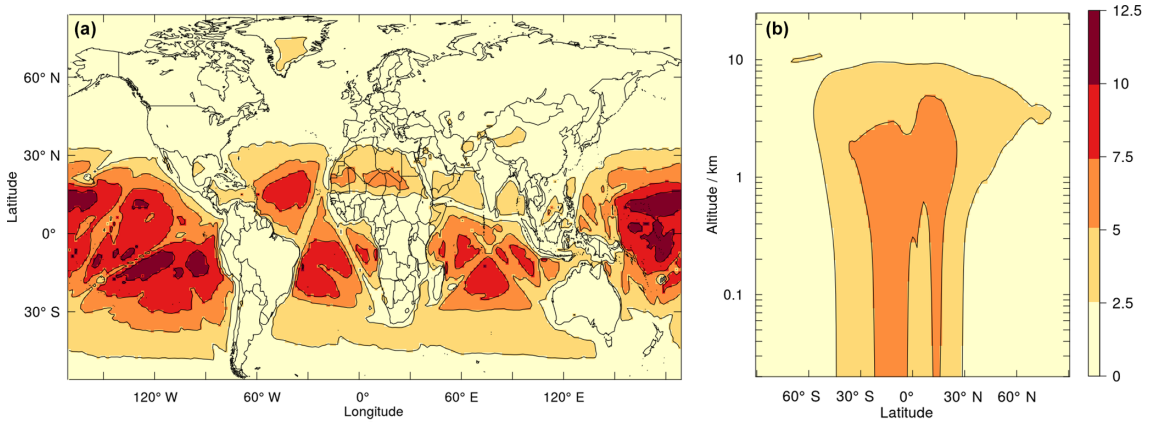


Figure 11. Annual mean percentage change in HO_2 concentrations from run 1 (relative to the base run) at the surface **(a)** and as a zonal mean **(b)**.

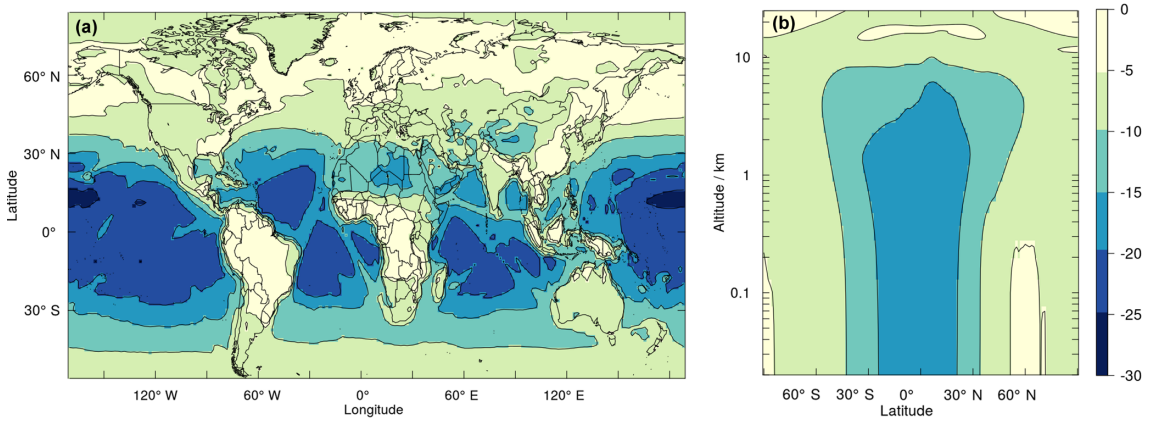


Figure 12. Annual mean percentage change in CH_3O_2 concentrations from run 1 (relative to the base run) at the surface **(a)** and as a zonal mean **(b)**.

There remains uncertainty in the tropospheric methanol budget (Khan et al., 2014; Millet et al., 2008), with models currently underestimating atmospheric methanol concentrations significantly. Müller et al. (2016) suggested that a scenario with high methanol yield from Reaction (R4) could reconcile models with observations, based on a model run with effectively $\gamma = 0.4$, which produced an additional 117 Tg year^{-1} of methanol. However, these simulations used the high value of k_4 reported by Bossolasco et al. (2014). If the preferred lower value reported more recently by Assaf et al. (2016) is used with $\gamma = 0.4$, we calculate methanol production via Reaction (R4c) to be 60 Tg year^{-1} and we estimate that a value of γ greater than 0.8 is needed to produce the amount of methanol necessary to reconcile models with observations. This is well beyond the uncertainty in the laboratory measurements of the branching of Reaction (R4) and highlights that missing sources of methanol must come from direct emissions (or re-emissions) or as yet-undiscovered photochemical sources, rather than from the reaction between OH and CH_3O_2. However, it has to be noted that so far the product branching of Reaction (R4) has only been measured at low pressure (50 Torr) by Assaf et al. (2017b). Calculations by Müller et al. (2016) suggest the presence of an association channel leading to the formation of a trioxide (CH_3OOOH) species, which might potentially decompose to methanol and molecular oxygen. As the stabilisation of association products is generally a pressure-dependent process, it is very important that future studies address the branching of Reaction (R4) at ambient pressure.

As the species affected by Reaction (R4) (HO_2, CH_3O_2 and CH_3OH) are all OH sinks, changes in their concentrations are accompanied by changes in k_{OH}. However, these are modest ($< 0.25\,s^{-1}$) in all the scenarios considered in this work, as shown in Figs. S13 and S14 in the Supplement. Whilst the reactions of OH with both HO_2 and CH_3O_2 have large rate constants ($> 1 \times 10^{-10}$ cm^3 molecules^{-1} s^{-1}), the general low abundance of these species (of the order of $\sim 10^8$ molecules cm^{-3}, as shown in Figs. S2 and S3) results in small changes to the total k_{OH}. On the other hand, whilst some of the changes in methanol concentrations arising from

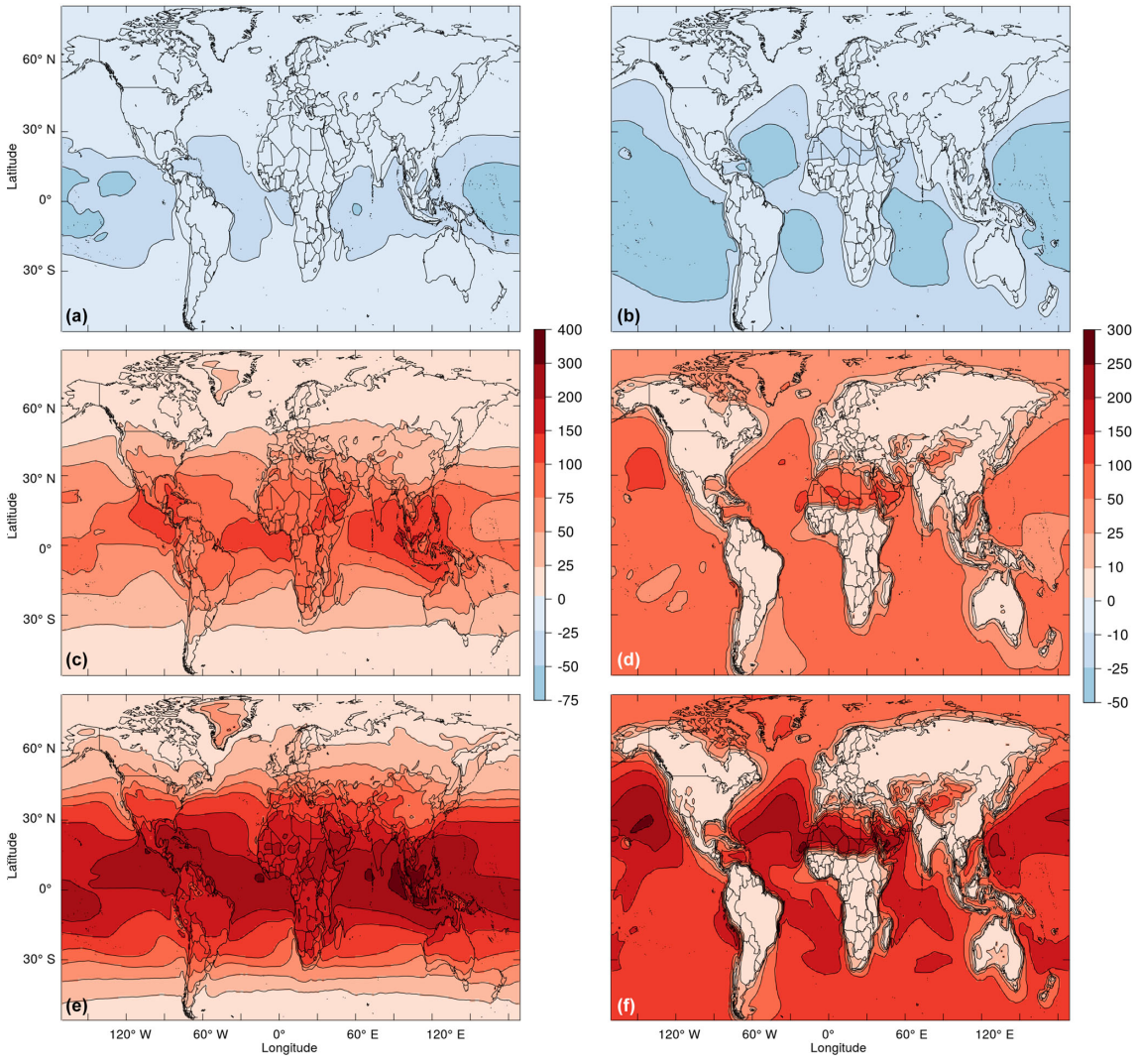


Figure 13. Annual mean changes in methanol abundances from run 1 ($\gamma = 0$, **a, b**), run 2 ($\gamma = 0.2$, **c, d**), and run 3 ($\gamma = 0.4$, **e, f**), relative to the base run. Changes are shown in absolute (in pptv, **a, c, e**) and relative terms (percentage change, **b, d, f**).

Reaction (R4) are significant (with increases up to 400 pptv in run 3, corresponding to $\sim 1 \times 10^{10}$ molecules cm^{-3}), the very small rate constant of its reaction with OH ($< 1 \times 10^{-12}$ cm^3 molecules^{-1} s^{-1}) leads to small contributions to k_{OH}. These results are consistent with the magnitude of the changes in k_{OH} calculated offline for all RO_2 radicals in Sect. 5.1. It remains to be seen whether any of the reaction products, or combination of products, of more complex RO_2 radicals with OH might have a significant impact on k_{OH}.

Results from this work agree with the box model calculations by Assaf et al. (2017b), indicating that the largest impacts of Reaction (R4) are on HO_2 and CH_3O_2 abundances. In addition, we show that these effects are not limited to the surface or the boundary layer but also extend well into the free troposphere.

6 Conclusions

The hydroxyl radical plays a pivotal role in the chemistry of the atmosphere. Its abundance determines the lifetime of most emitted compounds so that OH is often known as the "atmospheric detergent". However, our understanding of the chemistry and distribution of OH is far from complete. This study has examined the total tropospheric OH reactivity, k_{OH}, using the UM-UKCA chemistry-climate model. In the first instance, the model was evaluated against available measurements of known OH sinks. This comparison indicated that, whilst the model captured the abundances of a number of known OH sinks reasonably well in a variety of regions across the planet, the total modelled OH reactivity was generally much lower than observed, and there are significant biases in the model's ability to accurately simulate reactivity from NMHCs. This error was partly linked to the limited

NMHC chemistry included in chemistry-climate models like UM-UKCA.

Existing observations of the missing OH reactivity were used to develop a method to account for the missing OH sink in the model by introducing an additional reaction and OH sink species, X, in the model chemistry scheme. Observations of missing reactivity were correlated with underlying inputs into the model (emissions of VOCs, NO_x and aerosol precursors) through multiple linear regression analysis. The multiple linear regression fit highlighted correlation with both biogenic and anthropogenic emissions, consistent with observations of missing reactivity in remote and urban environments. The fitting routine also indicated a strong correlation of the missing reactivity with the emissions of particulate matter, perhaps pointing at OH loss processes involving condensed-phase particles that have been overlooked to date. The multiple linear regression indicated that the areas most affected by the missing reactivity would be tropical remote regions, where biogenic emissions dominate, as well as urban regions all over the globe, where anthropogenic emissions are significant. This result agrees with the type of environments in which missing reactivity has been observed. Our simulations showed that the largest impacts of the global missing OH reactivity were at the surface and in the boundary layer, where sink X accounted on average for 6 % of the total OH loss flux. Inclusion of X in the model led to decreases in mean OH abundances of 8.1 % at the surface, 5.6 % in the boundary layer and 1.6 % in the whole troposphere. Inclusion of missing reactivity, in the form of X, reduces and increases the lifetimes of OH and methane, respectively, by approximately 2 %. The inclusion of X modifies the global ozone burden only slightly (< 1 %) but has larger impacts on simulated surface ozone, particularly in the Northern Hemisphere. It has to be noted that, as no OH recycling was introduced following the initial oxidation of X, these results should be interpreted as an upper limit of the effects of the missing reactivity on the oxidising capacity of the troposphere.

Finally, we performed a series of model simulations including novel reactions of peroxy radicals with OH. These reactions have been recently confirmed (Bossolasco et al., 2014; Assaf et al., 2017) after being postulated to be potentially important in the marine boundary layer (Archibald et al., 2009). Using the UM-UKCA model, we have calculated that whilst these processes cannot account for the missing OH reactivity, they have important implications for the troposphere. Model runs including the reaction of the simplest peroxy radical, CH_3O_2, with OH indicated that this process is a major sink of peroxy radicals (with $[CH_3O_2]$ reduced by a third) and an important source of HO_2 radicals, the abundance of which increased by up to 12 % over remote oceans. These runs also show that, with the current understanding of the kinetics and product branching of this process, the reaction of CH_3O_2 with OH cannot be a major source of atmospheric methanol. As information on the kinetics and products of these reactions become available from laboratory studies, and given the impact they have on tropospheric radical species, we recommend their inclusion in atmospheric models.

There remain a number of challenges in understanding the chemistry of hydroxyl radicals in the atmosphere. We have shown, using the UM-UKCA model, that accounting for potential new sinks of OH and including a representation of the observed missing OH reactivity in the model has a relatively negligible impact on important long-lived atmospheric trace gases. However, we conclude that further studies are needed to identify the source and nature of the observed missing OH reactivity, in particular to understand whether it acts as a net OH sink (as we have included) or if it couples with other radical propagation cycles and so feeds back on OH itself. Lastly, as observations of the missing reactivity so far are largely limited to ground-level measurements in the Northern Hemisphere, further observations in the Southern Hemisphere as well as aircraft measurements both in the boundary layer and the free troposphere would provide additional constraints to the modelled oxidising capacity of the atmosphere.

Data availability. Data available upon request.

The Supplement related to this article is available online at https://doi.org/10.5194/acp-18-7109-2018-supplement.

Competing interests. The authors declare that they have no conflict of interest.

Acknowledgements. We thank the European Research Council for funding through the Atmospheric Chemistry-Climate Interactions (ACCI) project, no. 267760. We would also like to acknowledge the UKCA team at the UK Met Office for their help and support. This work used the ARCHER UK National Supercomputing Service (http://www.archer.ac.uk, last access: 18 May 2018). Alexander T. Archibald thanks the Kundert Walters Trust and NERC through NE/M00273X/1. The authors would also like to thank the three anonymous referees who reviewed this paper.

Edited by: Dwayne Heard
Reviewed by: three anonymous referees

References

Abraham, N. L., Archibald, A. T., Bellouin, N., Boucher, O., Braesicke, P., Bushell, A., Carslaw, K., Collins, B., Dalvi, M., Emmerson, K., Folberth, G., Haywood, J., Johnson, C., Kipling, Z., Macintyre, H., Mann, G., Telford, P., Merikanto, J., Morgenstern, O., Connor, F. O., Ord, C., Osprey, S., Pringle, K., Pyle, J.,

Rae, J., Reddington, C., Savage, N., Spracklen, D., Stier, P., and West, R.: Unified Model Documentation Paper No. 84: United Kingdom Chemistry and Aerosol (UKCA) Technical Description MetUM Version 8.4, 84, 74, 2012.

Archibald, A. T., Petit, A. S., Percival, C. J., Harvey, J. N., and Shallcross, D. E.: On the importance of the reaction between OH and RO_2 radicals, Atmos. Sci. Lett., 10, 102–108, https://doi.org/10.1002/asl.216, 2009.

Archibald, A. T., Cooke, M. C., Utembe, S. R., Shallcross, D. E., Derwent, R. G., and Jenkin, M. E.: Impacts of mechanistic changes on HO_x formation and recycling in the oxidation of isoprene, Atmos. Chem. Phys., 10, 8097–8118, https://doi.org/10.5194/acp-10-8097-2010, 2010.

Archibald, A. T., Levine, J. G., Abraham, N. L., Cooke, M. C., Edwards, P. M., Heard, D. E., Jenkin, M. E., Karunaharan, A., Pike, R. C., Monks, P. S., Shallcross, D. E., Telford, P. J., Whalley, L. K., and Pyle, J. A.: Impacts of HO_x regeneration and recycling in the oxidation of isoprene: Consequences for the composition of past, present and future atmospheres, Geophys. Res. Lett., 38, 1–6, https://doi.org/10.1029/2010GL046520, 2011.

Assaf, E., Song, B., Tomas, A., Schoemaecker, C., and Fittschen, C.: Rate Constant of the Reaction between CH_3O_2 Radicals and OH Radicals Revisited, J. Phys. Chem. A, 120, 8923–8932, 2016.

Assaf, E., Tanaka, S., Kajii, Y., Schoemaecker, C., and Fittschen, C.: Rate constants of the reaction of C_2-C_4 peroxy radicals with OH radicals, Chem. Phys. Lett., 684, 245–249, https://doi.org/10.1016/j.cplett.2017.06.062, 2017a.

Assaf, E., Sheps, L., Whalley, L. K., Heard, D. E., Tomas, A., Schoemaecker, C., and Fittschen, C.: The Reaction between CH_3O_2 and OH Radicals: Product Yields and Atmospheric Implications, Environ. Sci. Technol., 51, 2170–2177, 2017b.

Banerjee, A., Archibald, A. T., Maycock, A. C., Telford, P., Abraham, N. L., Yang, X., Braesicke, P., and Pyle, J. A.: Lightning NOx, a key chemistry-climate interaction: impacts of future climate change and consequences for tropospheric oxidising capacity, Atmos. Chem. Phys., 14, 9871–9881, https://doi.org/10.5194/acp-14-9871-2014, 2014.

Bossolasco, A., Faragó, E. P., Schoemaecker, C., and Fittschen, C.: Rate constant of the reaction between CH_3O_2 and OH radicals, Chem. Phys. Lett., 593, 7–13, https://doi.org/10.1016/j.cplett.2013.12.052, 2014.

Burkholder, J. B., Sander, S. P., Abbatt, J. P. D., Barker, J. R., Huie, R. E., Kolb, C. E., Kurylo, M. J., Orkin, V. L., Wilmouth, D. M., and Wine, P. H.: Chemical Kinetics and Photochemical Data for Use in Atmospheric Studies – Evaluation No. 18, JPL Publication 15–10, Jet Propulsion Laboratory, Pasadena, available at: http://jpldataeval.jpl.nasa.gov (last accessed 18 May 2018), 2015.

Di Carlo, P., Brune, W. H., Martinez, M., Harder, H., Lesher, R., Ren, X., Thornberry, T., Carroll, M. A., Young, V., Shepson, P. B., Riemer, D., Apel, E., and Campbell, C.: Missing OH Reactivity in a Forest: Evidence for Unknown Reactive Biogenic VOCs, Science, 304, 722–725, 2004.

Dolgorouky, C., Gros, V., Sarda-Esteve, R., Sinha, V., Williams, J., Marchand, N., Sauvage, S., Poulain, L., Sciare, J., and Bonsang, B.: Total OH reactivity measurements in Paris during the 2010 MEGAPOLI winter campaign, Atmos. Chem. Phys., 12, 9593–9612, https://doi.org/10.5194/acp-12-9593-2012, 2012.

Edwards, P. M., Evans, M. J., Furneaux, K. L., Hopkins, J., Ingham, T., Jones, C., Lee, J. D., Lewis, A. C., Moller, S. J., Stone, D., Whalley, L. K., and Heard, D. E.: OH reactivity in a South East Asian tropical rainforest during the Oxidant and Particle Photochemical Processes (OP3) project, Atmos. Chem. Phys., 13, 9497–9514, https://doi.org/10.5194/acp-13-9497-2013, 2013.

Ehhalt, D., Prather, M., Dentener, F., Derwent, R., Dlugokencky, E., Holland, E., Isaksen, I., Katima, J., Kirchhoff, V., Matson, P., Midgley, P., and Wang, M.: Atmospheric Chemistry and Greenhouse Gases, in Climate Change 2001: The Scientific Basis, Contribution of Working Group I to the Third Assessment Report of the Intergovernmental Panel on Climate Change, 239–287, 2001.

Elshorbany, Y. F., Kleffmann, J., Hofzumahaus, A., Kurtenbach, R., Wiesen, P., Brauers, T., Bohn, B., Dorn, H. P., Fuchs, H., Holland, F., Rohrer, F., Tillmann, R., Wegener, R., Wahner, A., Kanaya, Y., Yoshino, A., Nishida, S., Kajii, Y., Martinez, M., Kubistin, D., Harder, H., Lelieveld, J., Elste, T., Plass-Dlmer, C., Stange, G., Berresheim, H., and Schurath, U.: HO_x budgets during HO_xComp: A case study of HO_x chemistry under NO_x-limited conditions, J. Geophys. Res.-Atmos., 117, 1–16, https://doi.org/10.1029/2011JD017008, 2012.

Faragó, E. P., Schoemaecker, C., Viskolcz, B., and Fittschen, C.: Experimental determination of the rate constant of the reaction between $C_2H_5O_2$ and OH radicals, Chem. Phys. Lett., 619, 196–200, https://doi.org/10.1016/j.cplett.2014.11.069, 2015.

Fittschen, C., Whalley, L. K., and Heard, D. E.: The reaction of CH_3O_2 radicals with OH radicals: A neglected sink for CH_3O_2 in the remote atmosphere, Environ. Sci. Technol., 48, 7700–7701, https://doi.org/10.1021/es502481q, 2014.

Fuchs, H., Novelli, A., Rolletter, M., Hofzumahaus, A., Pfannerstill, E. Y., Kessel, S., Edtbauer, A., Williams, J., Michoud, V., Dusanter, S., Locoge, N., Zannoni, N., Gros, V., Truong, F., Sarda-Esteve, R., Cryer, D. R., Brumby, C. A., Whalley, L. K., Stone, D., Seakins, P. W., Heard, D. E., Schoemaecker, C., Blocquet, M., Coudert, S., Batut, S., Fittschen, C., Thames, A. B., Brune, W. H., Ernest, C., Harder, H., Muller, J. B. A., Elste, T., Kubistin, D., Andres, S., Bohn, B., Hohaus, T., Holland, F., Li, X., Rohrer, F., Kiendler-Scharr, A., Tillmann, R., Wegener, R., Yu, Z., Zou, Q., and Wahner, A.: Comparison of OH reactivity measurements in the atmospheric simulation chamber SAPHIR, Atmos. Meas. Tech., 10, 4023–4053, https://doi.org/10.5194/amt-10-4023-2017, 2017.

Guenther, A., Karl, T., Harley, P., Wiedinmyer, C., Palmer, P. I., and Geron, C.: Estimates of global terrestrial isoprene emissions using MEGAN (Model of Emissions of Gases and Aerosols from Nature), Atmos. Chem. Phys., 6, 3181–3210, https://doi.org/10.5194/acp-6-3181-2006, 2006.

Hansen, R. F., Griffith, S. M., Dusanter, S., Rickly, P. S., Stevens, P. S., Bertman, S. B., Carroll, M. A., Erickson, M. H., Flynn, J. H., Grossberg, N., Jobson, B. T., Lefer, B. L., and Wallace, H. W.: Measurements of total hydroxyl radical reactivity during CABINEX 2009 – Part 1: field measurements, Atmos. Chem. Phys., 14, 2923–2937, https://doi.org/10.5194/acp-14-2923-2014, 2014.

Hansen, R. F., Blocquet, M., Schoemaecker, C., Léonardis, T., Locoge, N., Fittschen, C., Hanoune, B., Stevens, P. S., Sinha, V., and Dusanter, S.: Intercomparison of the comparative reactivity method (CRM) and pump-probe technique for measuring total

OH reactivity in an urban environment, Atmos. Meas. Tech., 8, 4243–4264, https://doi.org/10.5194/amt-8-4243-2015, 2015.

Holzinger, R., Lee, A., Paw, K. T., and Goldstein, U. A. H.: Observations of oxidation products above a forest imply biogenic emissions of very reactive compounds, Atmos. Chem. Phys., 5, 67–75, https://doi.org/10.5194/acp-5-67-2005, 2005.

Ingham, T., Goddard, A., Whalley, L. K., Furneaux, K. L., Edwards, P. M., Seal, C. P., Self, D. E., Johnson, G. P., Read, K. A., Lee, J. D., and Heard, D. E.: A flow-tube based laser-induced fluorescence instrument to measure OH reactivity in the troposphere, Atmos. Meas. Tech., 2, 465–477, https://doi.org/10.5194/amt-2-465-2009, 2009.

Jenkin, M. E., Young, J. C., and Rickard, A. R.: The MCM v3.3.1 degradation scheme for isoprene, Atmos. Chem. Phys., 15, 11433–11459, https://doi.org/10.5194/acp-15-11433-2015, 2015.

Kaiser, J., Skog, K. M., Baumann, K., Bertman, S. B., Brown, S. B., Brune, W. H., Crounse, J. D., de Gouw, J. A., Edgerton, E. S., Feiner, P. A., Goldstein, A. H., Koss, A., Misztal, P. K., Nguyen, T. B., Olson, K. F., St. Clair, J. M., Teng, A. P., Toma, S., Wennberg, P. O., Wild, R. J., Zhang, L., and Keutsch, F. N.: Speciation of OH reactivity above the canopy of an isoprene-dominated forest, Atmos. Chem. Phys., 16, 9349–9359, https://doi.org/10.5194/acp-16-9349-2016, 2016.

Khan, M. A. H., Cooke, M. C., Utembe, S. R., Xiao, P., Derwent, R. G., Jenkin, M. E., Archibald, A. T., Maxwell, P., Morris, W. C., South, N., Percival, C. J., and Shallcross, D. E.: Reassessing the photochemical production of methanol from peroxy radical self and cross reactions using the STOCHEM-CRI global chemistry and transport model, Atmos. Environ., 99, 77–84, https://doi.org/10.1016/j.atmosenv.2014.09.056, 2014.

Kovacs, T. A. and Brune, W. H.: Total OH loss rate measurement, J. Atmos. Chem., 39, 105–122, https://doi.org/10.1023/A:1010614113786, 2001.

Kovacs, T. A., Brune, W. H., Harder, H., Martinez, M., Simpas, J. B., Frost, G. J., Williams, E., Jobson, T., Stroud, C., Young, V., Fried, A., and Wert, B.: Direct measurements of urban OH reactivity during Nashville SOS in summer 1999, J. Environ. Monit., 5, 68–74, https://doi.org/10.1039/b204339d, 2003.

Lawrence, M. G., Jöckel, P., and von Kuhlmann, R.: What does the global mean OH concentration tell us?, Atmos. Chem. Phys., 1, 37–49, https://doi.org/10.5194/acp-1-37-2001, 2001.

Lee, J. D., Young, J. C., Read, K. A., Hamilton, J. F., Hopkins, J. R., Lewis, A. C., Bandy, B. J., Davey, J., Edwards, P., Ingham, T., Self, D. E., Smith, S. C., Pilling, M. J., and Heard, D. E.: Measurement and calculation of OH reactivity at a United Kingdom coastal site, J. Atmos. Chem., 64, 53–76, https://doi.org/10.1007/s10874-010-9171-0, 2009.

Lelieveld, J., Peters, W., Dentener, F. J., and Krol, M. C.: Stability of tropospheric hydroxyl chemistry, J. Geophys. Res.-Atmos., 107, 4715, https://doi.org/10.1029/2002JD002272, 2002.

Lelieveld, J., Gromov, S., Pozzer, A., and Taraborrelli, D.: Global tropospheric hydroxyl distribution, budget and reactivity, Atmos. Chem. Phys., 16, 12477–12493, https://doi.org/10.5194/acp-16-12477-2016, 2016.

Liu, Y., Brito, J., Dorris, M. R., Rivera-Rios, J. C., Seco, R., Bates, K. H., Artaxo, P., Duvoisin, S., Keutsch, F. N., Kim, S., Goldstein, A. H., Guenther, A. B., Manzi, A. O., Souza, R. A. F., Springston, S. R., Watson, T. B., McKinney, K. A., and Martin, S. T.: Isoprene photochemistry over the Amazon rainforest, P. Natl. Acad. Sci. USA, 113, 6125–6130, https://doi.org/10.1073/pnas.1524136113, 2016.

Lou, S., Holland, F., Rohrer, F., Lu, K., Bohn, B., Brauers, T., Chang, C. C., Fuchs, H., Häseler, R., Kita, K., Kondo, Y., Li, X., Shao, M., Zeng, L., Wahner, A., Zhang, Y., Wang, W., and Hofzumahaus, A.: Atmospheric OH reactivities in the Pearl River Delta – China in summer 2006: measurement and model results, Atmos. Chem. Phys., 10, 11243–11260, https://doi.org/10.5194/acp-10-11243-2010, 2010.

Lu, K., Zhang, Y., Su, H., Brauers, T., Chou, C. C., Hofzumahaus, A., Liu, S. C., Kita, K., Kondo, Y., Shao, M., Wahner, A., Wang, J., Wang, X., and Zhu, T.: Oxidant ($O_3 + NO_2$) production processes and formation regimes in Beijing, J. Geophys. Res., 115, D07303, https://doi.org/10.1029/2009JD012714, 2010.

Mao, J., Ren, X., Brune, W. H., Olson, J. R., Crawford, J. H., Fried, A., Huey, L. G., Cohen, R. C., Heikes, B., Singh, H. B., Blake, D. R., Sachse, G. W., Diskin, G. S., Hall, S. R., and Shetter, R. E.: Airborne measurement of OH reactivity during INTEX-B, Atmos. Chem. Phys., 9, 163–173, https://doi.org/10.5194/acp-9-163-2009, 2009.

Mao, J., Ren, X., Chen, S., Brune, W. H., Chen, Z., Martinez, M., Harder, H., Lefer, B., Rappenglück, B., Flynn, J., and Leuchner, M.: Atmospheric oxidation capacity in the summer of Houston 2006: Comparison with summer measurements in other metropolitan studies, Atmos. Environ., 44, 4107–4115, https://doi.org/10.1016/j.atmosenv.2009.01.013, 2010.

Mao, J., Ren, X., Zhang, L., Van Duin, D. M., Cohen, R. C., Park, J.-H., Goldstein, A. H., Paulot, F., Beaver, M. R., Crounse, J. D., Wennberg, P. O., DiGangi, J. P., Henry, S. B., Keutsch, F. N., Park, C., Schade, G. W., Wolfe, G. M., Thornton, J. A., and Brune, W. H.: Insights into hydroxyl measurements and atmospheric oxidation in a California forest, Atmos. Chem. Phys., 12, 8009–8020, https://doi.org/10.5194/acp-12-8009-2012, 2012.

Martinez, M., Harder, H., Kubistin, D., Rudolf, M., Bozem, H., Eerdekens, G., Fischer, H., Klüpfel, T., Gurk, C., Königstedt, R., Parchatka, U., Schiller, C. L., Stickler, A., Williams, J., and Lelieveld, J.: Hydroxyl radicals in the tropical troposphere over the Suriname rainforest: airborne measurements, Atmos. Chem. Phys., 10, 3759–3773, https://doi.org/10.5194/acp-10-3759-2010, 2010.

Michoud, V., Hansen, R. F., Locoge, N., Stevens, P. S., and Dusanter, S.: Detailed characterizations of the new Mines Douai comparative reactivity method instrument via laboratory experiments and modeling, Atmos. Meas. Tech., 8, 3537–3553, https://doi.org/10.5194/amt-8-3537-2015, 2015.

Millet, D. B., Jacob, D. J., Custer, T. G., de Gouw, J. A., Goldstein, A. H., Karl, T., Singh, H. B., Sive, B. C., Talbot, R. W., Warneke, C., and Williams, J.: New constraints on terrestrial and oceanic sources of atmospheric methanol, Atmos. Chem. Phys., 8, 6887–6905, https://doi.org/10.5194/acp-8-6887-2008, 2008.

Mogensen, D., Smolander, S., Sogachev, A., Zhou, L., Sinha, V., Guenther, A., Williams, J., Nieminen, T., Kajos, M. K., Rinne, J., Kulmala, M., and Boy, M.: Modelling atmospheric OH-reactivity in a boreal forest ecosystem, Atmos. Chem. Phys., 11, 9709–9719, https://doi.org/10.5194/acp-11-9709-2011, 2011.

Morgenstern, O., Braesicke, P., O'Connor, F. M., Bushell, A. C., Johnson, C. E., Osprey, S. M., and Pyle, J. A.: Evaluation of the new UKCA climate-composition model –

Part 1: The stratosphere, Geosci. Model Dev., 2, 43–57, https://doi.org/10.5194/gmd-2-43-2009, 2009.

Müller, J.-F., Liu, Z., Nguyen, V. S., Stavrakou, T., Harvey, J. N., and Peeters, J.: The reaction of methyl peroxy and hydroxyl radicals as a major source of atmospheric methanol, Nature Commun., 7, 13213, https://doi.org/10.1038/ncomms13213, 2016.

Naik, V., Voulgarakis, A., Fiore, A. M., Horowitz, L. W., Lamarque, J.-F., Lin, M., Prather, M. J., Young, P. J., Bergmann, D., Cameron-Smith, P. J., Cionni, I., Collins, W. J., Dalsøren, S. B., Doherty, R., Eyring, V., Faluvegi, G., Folberth, G. A., Josse, B., Lee, Y. H., MacKenzie, I. A., Nagashima, T., van Noije, T. P. C., Plummer, D. A., Righi, M., Rumbold, S. T., Skeie, R., Shindell, D. T., Stevenson, D. S., Strode, S., Sudo, K., Szopa, S., and Zeng, G.: Preindustrial to present-day changes in tropospheric hydroxyl radical and methane lifetime from the Atmospheric Chemistry and Climate Model Intercomparison Project (ACCMIP), Atmos. Chem. Phys., 13, 5277–5298, https://doi.org/10.5194/acp-13-5277-2013, 2013.

Nakashima, Y., Kato, S., Greenberg, J., Harley, P., Karl, T., Turnipseed, A., Apel, E., Guenther, A., Smith, J., and Kajii, Y.: Total OH reactivity measurements in ambient air in a southern Rocky mountain ponderosa pine forest during BEACHON-SRM08 summer campaign, Atmos. Environ., 85, 1–8, https://doi.org/10.1016/j.atmosenv.2013.11.042, 2014.

Nölscher, A. C., Williams, J., Sinha, V., Custer, T., Song, W., Johnson, A. M., Axinte, R., Bozem, H., Fischer, H., Pouvesle, N., Phillips, G., Crowley, J. N., Rantala, P., Rinne, J., Kulmala, M., Gonzales, D., Valverde-Canossa, J., Vogel, A., Hoffmann, T., Ouwersloot, H. G., Vilà-Guerau de Arellano, J., and Lelieveld, J.: Summertime total OH reactivity measurements from boreal forest during HUMPPA-COPEC 2010, Atmos. Chem. Phys., 12, 8257–8270, https://doi.org/10.5194/acp-12-8257-2012, 2012.

Nölscher, A. C., Yañez-Serrano, A. M., Wolff, S., de Araujo, A. C., Lavrič, J. V, Kesselmeier, J., and Williams, J.: Unexpected seasonality in quantity and composition of Amazon rainforest air reactivity., Nature Commun., 7, 10383, https://doi.org/10.1038/ncomms10383, 2016.

O'Connor, F. M., Johnson, C. E., Morgenstern, O., Abraham, N. L., Braesicke, P., Dalvi, M., Folberth, G. A., Sanderson, M. G., Telford, P. J., Voulgarakis, A., Young, P. J., Zeng, G., Collins, W. J., and Pyle, J. A.: Evaluation of the new UKCA climate-composition model – Part 2: The Troposphere, Geosci. Model Dev., 7, 41–91, https://doi.org/10.5194/gmd-7-41-2014, 2014

Ren, X., Harder, H., Martinez, M., Lesher, R. L., Oliger, A., Shirley, T., Adams, J., Simpas, J. B., and Brune, W. H.: HO_x concentrations and OH reactivity observations in New York City during PMTACS-NY2001, Atmos. Environ., 37, 3627–3637, https://doi.org/10.1016/S1352-2310(03)00460-6, 2003a.

Ren, X., Harder, H., Martinez, M., Lesher, R. L., Oliger, A., Simpas, J. B., Brune, W. H., Schwab, J. J., Demerjian, K. L., He, Y., Zhou, X., and Gao, H.: OH and HO_2 chemistry in the urban atmosphere of New York City, Atmos. Environ., 37, 3639–3651, https://doi.org/10.1016/S1352-2310(03)00459-X, 2003b.

Ren, X., Brune, W. H., Cantrell, C. A., Edwards, G. D., Shirley, T., Metcalf, A. R., and Lesher, R. L.: Hydroxyl and peroxy radical chemistry in a rural area of central Pennsylvania: Observations and model comparisons, J. Atmos. Chem., 52, 231–257, https://doi.org/10.1007/s10874-005-3651-7, 2005.

Ren, X., Brune, W. H., Mao, J., Mitchell, M. J., Lesher, R. L., Simpas, J. B., Metcalf, A. R., Schwab, J. J., Cai, C., Li, Y., Demerjian, K. L., Felton, H. D., Boynton, G., Adams, A., Perry, J., He, Y., Zhou, X., and Hou, J.: Behavior of OH and HO_2 in the winter atmosphere in New York City, Atmos. Environ., 40, 252–263, https://doi.org/10.1016/j.atmosenv.2005.11.073, 2006a.

Ren, X., Brune, W. H., Oliger, A., Metcalf, A. R., Simpas, J. B., Shirley, T., Schwab, J. J., Bai, C., Roychowdhury, U., Li, Y., Cai, C., Demerjian, K. L., He, Y., Zhou, X., Gao, H., and Hou, J.: OH, HO_2, and OH reactivity during the PMTACS-NY Whiteface Mountain 2002 campaign: Obervations and model comparison, J. Geophys. Res.-Atmos., 111, 1–12, https://doi.org/10.1029/2005JD006126, 2006b.

Safieddine, S. A., Heald, C. L., and Henderson, B. H.: The global nonmethane reactive organic carbon budget: A modeling perspective, Geophys. Res. Lett., 44, 3897–3906, https://doi.org/10.1002/2017GL072602, 2017.

Shirley, T. R., Brune, W. H., Ren, X., Mao, J., Lesher, R., Cardenas, B., Volkamer, R., Molina, L. T., Molina, M. J., Lamb, B., Velasco, E., Jobson, T., and Alexander, M.: Atmospheric oxidation in the Mexico City Metropolitan Area (MCMA) during April 2003, Atmos. Chem. Phys., 6, 2753–2765, https://doi.org/10.5194/acp-6-2753-2006, 2006.

Sinha, V., Williams, J., Crowley, J. N., and Lelieveld, J.: The Comparative Reactivity Method – a new tool to measure total OH Reactivity in ambient air, Atmos. Chem. Phys., 8, 2213–2227, https://doi.org/10.5194/acp-8-2213-2008, 2008.

Sinha, V., Williams, J., Lelieveld, J., Ruuskanen, T. M., Kajos, M. K., Patokoski, J., Hellen, H., Hakola, H., Mogensen, D., Boy, M., Rinne, J., and Kulmala, M.: OH reactivity measurements within a boreal forest: Evidence for unknown reactive emissions, Environ. Sci. Technol., 44, 6614–6620, https://doi.org/10.1021/es101780b, 2010.

Sinha, V., Williams, J., Diesch, J. M., Drewnick, F., Martinez, M., Harder, H., Regelin, E., Kubistin, D., Bozem, H., Hosaynali-Beygi, Z., Fischer, H., Andrés-Hernández, M. D., Kartal, D., Adame, J. A., and Lelieveld, J.: Constraints on instantaneous ozone production rates and regimes during DOMINO derived using in-situ OH reactivity measurements, Atmos. Chem. Phys., 12, 7269–7283, https://doi.org/10.5194/acp-12-7269-2012, 2012.

Squire, O. J., Archibald, A. T., Griffiths, P. T., Jenkin, M. E., Smith, D., and Pyle, J. A.: Influence of isoprene chemical mechanism on modelled changes in tropospheric ozone due to climate and land use over the 21st century, Atmos. Chem. Phys., 15, 5123–5143, https://doi.org/10.5194/acp-15-5123-2015, 2015.

Stevenson, D. S., Dentener, F. J., Schultz, M. G., Ellingsen, K., van Noije, T. P. C., Wild, O., Zeng, G., Amann, M., Atherton, C. S., Bell, N., Bergmann, D. J., Bey, I., Butler, T., Cofala, J., Collins, W. J., Derwent, R. G., Doherty, R. M., Drevet, J., Eskes, H. J., Fiore, A. M., Gauss, M., Hauglustaine, D. A., Horowitz, L. W., Isaksen, I. S. A., Krol, M. C., Lamarque, J. F., Lawrence, M. G., Montanaro, V., Müller, J. F., Pitari, G., Prather, M. J., Pyle, J. A., Rast, S., Rodriquez, J. M., Sanderson, M. G., Savage, N. H., Shindell, D. T., Strahan, S. E., Sudo, K., and Szopa, S.: Multimodel ensemble simulations of present-day and near-future tropospheric ozone, J. Geophys. Res.-Atmos., 111, D08301, https://doi.org/10.1029/2005JD006338, 2006.

Voulgarakis, A., Naik, V., Lamarque, J.-F., Shindell, D. T., Young, P. J., Prather, M. J., Wild, O., Field, R. D., Bergmann, D., Cameron-Smith, P., Cionni, I., Collins, W. J., Dalsøren, S. B., Doherty, R. M., Eyring, V., Faluvegi, G., Folberth, G. A., Horowitz, L. W., Josse, B., MacKenzie, I. A., Nagashima, T., Plummer, D. A., Righi, M., Rumbold, S. T., Stevenson, D. S., Strode, S. A., Sudo, K., Szopa, S., and Zeng, G.: Analysis of present day and future OH and methane lifetime in the ACCMIP simulations, Atmos. Chem. Phys., 13, 2563–2587, https://doi.org/10.5194/acp-13-2563-2013, 2013.

Whalley, L. K., Stone, D., Bandy, B., Dunmore, R., Hamilton, J. F., Hopkins, J., Lee, J. D., Lewis, A. C., and Heard, D. E.: Atmospheric OH reactivity in central London: observations, model predictions and estimates of in situ ozone production, Atmos. Chem. Phys., 16, 2109–2122, https://doi.org/10.5194/acp-16-2109-2016, 2016.

Yan, C., Kocevska, S., and Krasnoperov, L. N.: Kinetics of the Reaction of CH_3O_2 Radicals with OH Studied over the 292–526 K Temperature Range, J. Phys. Chem. A, 120, 6111–6121, https://doi.org/10.1021/acs.jpca.6b04213, 2016.

Yang, Y., Shao, M., Wang, X., Nölscher, A. C., Kessel, S., Guenther, A., and Williams, J.: Towards a quantitative understanding of total OH reactivity: A review, Atmos. Environ., 134, 147–161, https://doi.org/10.1016/j.atmosenv.2016.03.010, 2016.

Yang, Y., Shao, M., Keßel, S., Li, Y., Lu, K., Lu, S., Williams, J., Zhang, Y., Zeng, L., Nölscher, A. C., Wu, Y., Wang, X., and Zheng, J.: How the OH reactivity affects the ozone production efficiency: case studies in Beijing and Heshan, China, Atmos. Chem. Phys., 17, 7127–7142, https://doi.org/10.5194/acp-17-7127-2017, 2017.

Young, P. J., Archibald, A. T., Bowman, K. W., Lamarque, J.-F., Naik, V., Stevenson, D. S., Tilmes, S., Voulgarakis, A., Wild, O., Bergmann, D., Cameron-Smith, P., Cionni, I., Collins, W. J., Dalsøren, S. B., Doherty, R. M., Eyring, V., Faluvegi, G., Horowitz, L. W., Josse, B., Lee, Y. H., MacKenzie, I. A., Nagashima, T., Plummer, D. A., Righi, M., Rumbold, S. T., Skeie, R. B., Shindell, D. T., Strode, S. A., Sudo, K., Szopa, S., and Zeng, G.: Preindustrial to end 21st century projections of tropospheric ozone from the Atmospheric Chemistry and Climate Model Intercomparison Project (ACCMIP), Atmos. Chem. Phys., 13, 2063–2090, https://doi.org/10.5194/acp-13-2063-2013, 2013.

Zannoni, N., Gros, V., Lanza, M., Sarda, R., Bonsang, B., Kalogridis, C., Preunkert, S., Legrand, M., Jambert, C., Boissard, C., and Lathiere, J.: OH reactivity and concentrations of biogenic volatile organic compounds in a Mediterranean forest of downy oak trees, Atmos. Chem. Phys., 16, 1619–1636, https://doi.org/10.5194/acp-16-1619-2016, 2016.

Zannoni, N., Gros, V., Sarda Esteve, R., Kalogridis, C., Michoud, V., Dusanter, S., Sauvage, S., Locoge, N., Colomb, A., and Bonsang, B.: Summertime OH reactivity from a receptor coastal site in the Mediterranean Basin, Atmos. Chem. Phys., 17, 12645–12658, https://doi.org/10.5194/acp-17-12645-2017, 2017.



https://dspace.org/

Global modelling of the total OH reactivity: investigations on the “missing” OH sink and its atmospheric implications

Ferracci, Valerio; Heimann, Ines; Abraham, N. Luke; Pyle, John A.; Archibald, Alexander T.

2018-05-24

European Geosciences Union (EGU) / Copernicus Publications

https://doi.org/10.5194/acp-18-7109-2018

Valerio Ferracci, Ines Heimann, N. Luke Abraham, et al. Global modelling of the total OH reactivity: investigations on the “missing” OH sink and its atmospheric implications. Atmospheric Chemistry and Physics, 2018, Volume 18, Issue 10, pp7109-7129

Downloaded from a DSpace repository. https://dspace.org/